Bioactive Materials 22 (2023) 404–422

Contents lists available at ScienceDirect

Bioactive Materials

journal homepage: www.keaipublishing.com/en/journals/bioactive-materials

Remodeling of the osteoimmune microenvironment after biomaterials implantation in murine tibia: Single-cell transcriptome analysis

Jia Li, Congrui Zhao, Yangbo Xu, Lu Song, Yanqi Chen, Yuzi Xu, Yang Ma, Siyuan Wang, Antian Xu **, Fuming He *

Department of Prosthodontics, Stomatology Hospital, School of Stomatology, Zhejiang University School of Medicine, Zhejiang Provincial Clinical Research Center for Oral Diseases, Key Laboratory of Oral Biomedical Research of Zhejiang Province, Cancer Center of Zhejiang University, Hangzhou, China

ARTICLE INFO

Keywords:
Osteoimmunology
Neutrophil
Implant
Osseointegration
Single-cell transcriptomics

ABSTRACT

Osseointegration seems to be a foreign body reaction equilibrium due to the complicated interactions between the immune and skeletal systems. The heterogeneity of the osteoimmune microenvironment in the osseointegration of implant materials remains elusive. Here, a single-cell study involving 40043 cells is conducted, and a total of 10 distinct cell clusters are identified from five different groups. A preliminary description of the osteoimmune microenvironment revealed the diverse cellular heterogeneity and dynamic changes modulated by implant properties. The increased immature neutrophils, Ly6C $^{+}$ CCR2^{hi} monocytes, and S100a8^{hi} macrophages induce an aggressive inflammatory response and eventually lead to the formation of fibrous capsule around the stainless steel implant. The enrichment of mature neutrophils, FcgR1^{hi} and differentiated immunomodulatory macrophages around the titanium implant indicates favorable osseointegration under moderate immune response. Neutrophil-depletion mice are conducted to explore the role of neutrophils in osseointegration. Neutrophils may improve bone formation by enhancing the recruitment of BMSCs via the CXCL12/CXCR3 signal axis. These findings contribute to a better knowledge of osteoimmunology and are valuable for the design and modification of 'osteoimmune-smart' biomaterials in the bone regeneration field.

1. Introduction

There is rapidly-growing demand for innovative clinical orthopedic implants for bone diseases, traditional orthopedic implants include but are not limited to prostheses and fixators are mainly made of inert stainless steel and titanium or its alloys [1]. In recent years, the concept of 'osteoimmunology' has been emphasized, and osseointegration seems to be a foreign body reaction (FBR) equilibrium due to its complicated mechanisms controlling the immune and skeletal systems [2]. The osteoimmune environment created by biomaterials determines the results of bone regeneration and the clinical outcomes of implants. However, there is still a lack of full comprehension of the osteoimmune responses induced by materials. Current understanding of heterogeneity and dynamic changes of immune cells is still limited to traditional definitions, such as macrophage polarization with classical M1/M2 macrophage nomenclature, and corresponding N1/N2 neutrophils typing [3–6]. This study aims at exploring the cellular heterogeneity and dynamics within the implant materials mediated-osteoimmune

Abbreviations: BMP2, Bone Morphogenetic Proteins 2; RUNX2, Runt-related Transcription Factor 2; IL-1β, Interleukin-1 beta; IFN-γ, Interferon-gamma; MHC, Major Histocompatibility Complex; TNFα, Tumor Necrosis Factor-alpha; RANKL, Nuclear Factor B receptor Activator Ligand; OPG, Osteoprotegerin; TLR, Toll Like Receptor; SDF-1α, Stromal Cell-derived Factor-1 alpha; CXCL12, Chemokine (C-X-C mode) Ligand 12; CXCR, CXC Chemokine Receptor; MIP, Macrophage inflammatory cytokines; MPO, Myeloperoxidase; NE, Neutrophil Elastase; TRAP, Tartrate Resistant Acid Phosphatase; NOD, Nucleotide Binding Oligomerization Domain; NF-κB, Nuclear Factor Kappa-light-chain-enhancer of Activated B cells; STAT, Signal Transduction and Transcription Activator; S100a8, S100 Calcium Binding Protein A8; FcgR, Fc Gamma Receptor.

Peer review under responsibility of KeAi Communications Co., Ltd.

* Corresponding author. Department of Prosthodontics, The Affiliated Stomatology Hospital, Zhejiang University School of Medicine, No.166, QiuTao Rd(N), Hangzhou, 310006, China.

** Corresponding author. Department of Prosthodontics, The Affiliated Stomatology Hospital, Zhejiang University School of Medicine, No.166, QiuTao Rd(N), Hangzhou, 310006, China.

E-mail addresses: xuantian@zju.edu.cn (A. Xu), hfm@zju.edu.cn (F. He).

https://doi.org/10.1016/j.bioactmat.2022.10.009
Received 4 July 2022; Received in revised form 28 September 2022; Accepted 5 October 2022

microenvironment and providing feasible strategies for the design of 'osteoimmune-smart' implant materials in clinical application.

Biomaterials with appropriate modification strategies can induce an immune-mediated process that contributes to better osseointegration [7]. The characteristics of biomaterials (size, topography, roughness, hydrophilicity, iron release, etc.) play significant roles in guiding immunoreactions and cell behaviors [8–10]. Most studies have focused on macrophages due to their remarkable plasticity and functional phenotype [11,12]. For instance, strontium (Sr) ions modification of titanium implants was recently reported to have an immunomodulatory effect on macrophages. SR implants enhanced osseointegration accompanied by more alternatively M2 polarization and less classically activated M1 infiltration via the ERK pathway [13]. Currently, increasing studies have indicated that the modification of biomaterial can also regulate other immunocytes. Sr-incorporated scaffolds promote neutrophils to N2 polarization, thus enhancing the resolution of inflammation and promoting angiogenesis and tissue regeneration [14]. Different titanium-based surfaces induce dendritic cells (DCs) of varying maturity and have different abilities to promote the osteogenic differentiation of osteoblasts [15]. What is more, biomaterial scaffolds induced a pro-regenerative microenvironment and have implicated mTOR-dependent $CD4^+$ Th2 cells, in the process of traumatic muscle recovery [16]. Previous studies have often focused on the influence of certain types of immune cells on bone repair. However, cell-cell communication in osteoimmune microenvironment is sophisticated and orchestrated by diverse influencing factors. The microenvironment needs to be taken as a whole and analyzed jointly by multiple cells.

With the development of single-cell transcriptome (scRNA-seq), it enables to explore cell heterogeneity, cell function, and cell communication *in vivo* [17], providing a comprehensive understanding of bone immune response to implant materials. In this study, scRNA-seq was used to profile cells around implant materials with different osteogenic properties to unveil the immune microenvironment involved in biomaterial-mediated bone healing. Sandblasted, large grit and acid-etched (SLA), strontium incorporated SLA (SR), polished titanium (PT), and medical stainless steel (SS) were used to elucidate osteoimmune microenvironment and cellular heterogeneity in regulating bone regenerative process. To our knowledge, it is the first study mapping the overall osteoimmune microenvironment around bone-implant via scRNA-seq.

2. Materials and methods

2.1. Sample preparation

The medical stainless steel and commercially pure titanium slices were prepared by Zhejiang Guangci Medical Appliance Co., Ltd, Ningbo, China. The samples for *in vivo* study were rods shaped 1 mm in diameter and 2.5 mm in length, and *in vitro* cell culture were round slices with 28 mm in diameter and 1 mm in thickness. Titanium samples were prepared as previously reported [18]. Briefly, the samples were divided into four groups: (1) SS: the stainless steel samples were sequentially polished with 280-, 600-, 1200-grid silicon carbide papers (CarbiMet, Buehler). (2) PT: the titanium samples were sequentially polished as the SS sample. (3) SLA: the PT samples were treated with a solution of HF/HNO_3 and HCl/H_2SO_4. (4) SR: the SLA samples were further hydrothermally treated with $Sr(OH)_2$ (99.5% purity, Sigma-Aldrich) solution. Before the following procedures, all implants were sterilized by UV irradiation.

2.2. Surface characteristic

The surface morphology was observed by field-emission scanning electron microscope (FE-SEM, Nova Nano 450, Thermo FEI, USA). The roughness of samples was detected by a three-dimensional interference microscope (NT9100, Veeco, USA). The hydrophilicity of the samples was assessed by static contact angle via a Contact Angle Meter (Dropmeter 100P, HAISHU, China). The elemental compositions and mappings (Cr, Ni, Ti, and Sr) of the surfaces were determined by energy-dispersive X-ray spectrometry (EDS, Nova Nano 450, Thermo FEI, USA). The crystalline phase of samples was characterized by X-ray diffractometry (XRD, D/MAX 2550/PC, RIGAKU Industrial Corporation, Japan). As for iron release, four kinds of round slices were immersed in 1 mL phosphate buffer (PBS) in a 37 °C incubator, and the leaching solution was collected at 1, 3, 7, 14, and 21 days. Ion concentrations were measured with an electronically coupled plasma mass spectrometer (ICP-MS, XSeries, Thermo Scientific, USA). At least three samples were used for detection of surface characteristic.

2.3. Implantation model

All the experiments were approved by the Institutional Animal Care and Use Committee of Zhejiang University, Hangzhou, China (ZJU20220152). C57BL/6 male mice at ages from 6 to 8 weeks (Zhejiang Academy of Medical Sciences) were used. The mice were housed under 25 °C with a 12 h light/dark cycle and were allowed free access to food and water. Mice received an intraperitoneal injection of 5% chloral hydrate (0.66 mL/100 g, C104202, Aladdin) and local injection of 2% lidocaine (Shiyao Yinhu Pharmaceutical Co., Ltd., China) before implantation. After shaving and disinfection of implantation areas, the skin above the proximal metaphysis of the tibiae was dissected longitudinally and the soft tissues were stripped to expose the underlying bone tissue. A hole was drilled with a 1 mL syringe needle, implants were inserted into the left and right tibias, and the SHAM group received no implant as a control. The periosteum and skin were sutured postoperatively. Penicillin (100,000 U/d) was injected intramuscularly into the mice instantly. After submerged healing, mice were sacrificed with a lethal dose of anesthetic. Tibiae were harvested after dissecting and cleaning of surrounding tissue.

2.4. Histomorphometric assessment

To evaluate the new bone formation, the proximal tibiae containing the implants were retrieved and fixed in 10% buffered formalin (Solarbio, China) for 3 days. Specimens were successively dehydrated with 75%, 85%, 95%, and 100% alcohol before being embedded with polymethyl-methacrylate (PMMA). After polymerization, slices of 200 μm thickness were prepared along the longitudinal axis of the implant and then polished sequentially with sandpapers to a final thickness of 40 μm. The non-decalcified sections were then stained with methylene blue and acid fuchsin. A bright-field microscope (DM4000; Lecia, German) and an image analysis system (Image-Pro Plus 6.0) were used to capture the images and analyze the histological phenotypes. The bone-implant contact ratio (BIC %) was calculated as the linear percentage of direct bone-implant contact to the total implant interface in cancellous bone.

2.5. Immunohistochemistry

For immunohistochemical staining, the tibiae were fixed in 4% paraformaldehyde (PFA, Servicebio) for 24 h and decalcified with 10% ethylene diamine tetraacetic acid (EDTA, Servicebio) for 3 weeks. The decalcified bone blocks were dehydrated in graded series of ethanol, embedded in paraffin, and cut into 4 μm slices perpendicular to the long axis of the implants. Subsequently, bone slices were incubated with 3% hydrogen peroxide for 10 min and then placed in an autoclave at 121 °C for 15 min in sodium citrate buffer. The slices were incubated with BMP2 antibody (ab2843887, Abcam, 1:100) and RUNX2 antibody (ab236639, Abcam, 1:100). As for osteoclastogenesis detection, the sections were stained with a TRAP histochemical staining kit and photographed by microscopy. Five random fields of each section were included for analysis.

2.6. Specimen harvest for bulk RNA-seq and single cell RNA-seq

2.6.1. Cell harvesting and processing

After three days of implantation, tibiae (the proximal metaphysis, cylinder, 5 mm) with implants inside were harvested by cutting off the skin and removing soft tissues. Bone marrow cells were flushed with Hank's balanced salt solution (HBSS, Sigma) containing 10% 0.1 μM EDTA. Implants were poked out and digested with enzymes mix containing 1 mg/mL dispase (17105041, Gibco), 1 mg/mL collagenase II (40508ES60, Yeasen), and 0.15 μM DNase I (EN0521, Thermo Fisher) in HBSS for 30 min at 37 °C. Then, dissociated cells from bone marrow and implant surfaces were filtered through a 70-μm filter, centrifuged at 1500 rpm. for 5 min, and then resuspended in 5 mL of red blood cell lysis buffer for 5 min on ice. Neutralization was achieved with a 10 mL cell suspension medium. The cell suspension was centrifuged, gently washed twice by HBSS, and then filtered through a 40-μm filter and stored in an icebox. Lastly, the bulk RNA and 10x Genomics Single-Cell Protocol were carried out by Gene Denovo Biotechnology Co. (Guangzhou, China), respectively.

2.6.2. RNA-seq analysis

Total RNA was extracted from dissociated cells using a Trizol reagent kit (Invitrogen, USA) according to the manufacturer's protocol. RNA quality was assessed on an Agilent 2100 Bioanalyzer (Agilent Technologies, USA) and checked using RNase-free agarose gel electrophoresis. After total RNA was extracted, eukaryotic mRNA was enriched by Oligo (dT) beads, while prokaryotic mRNA was enriched by removing RNA via Ribo-ZeroTM Magnetic Kit (Epicentre, USA). Then the enriched mRNA was fragmented into short fragments using fragmentation buffer and reverse transcribed into cDNA with random primers. Second-strand cDNA was synthesized by DNA polymerase I, RNase H, dNTP, and buffer. Then the cDNA fragments were purified with a QiaQuick PCR extraction kit (Qiagen, The Netherlands), end-repaired, poly(A) added, and ligated to Illumina sequencing adapters. The ligation products were size selected by agarose gel electrophoresis, PCR amplified and sequenced using Illumina HiSeq2500.

2.6.3. Single-cell RNA-seq

Bone marrow cells around implants were collected as previously described, single cells were encapsulated in water-in-oil emulsion along with gel beads coated with unique molecular barcodes using the 10X Genomics Chromium Single-Cell Platform. For single-cell RNA library generation, the sequencing was performed using an Illumina R1, a 16 nt 10x Barcode, a 10 nt Unique Molecular Identifier (UMI), and a poly-dT primer sequence. Incubation of the GEMs then produces barcoded, full-length cDNA from poly-adenylated mRNA. Full-length, barcoded cDNA is then amplified by PCR to generate sufficient mass for library construction.

After removing unwanted cells from the dataset, we employed a global-scaling normalization method "LogNormalize" that normalizes the gene expression measurements for each cell by the total expression, multiplies this by a scale factor (10000 by default), and log-transforms the results. ScaleData function of Seurat was used to normalize the data, so that the mean expression level of genes in each cell was equal to 0 and the variance was equal to 1, and some highly expressed genes were excluded to play a leading role in downstream analysis. The raw counts were then used for a differential expression gene (DEG) analysis using edgeR (R version 3.1.2) with FDR <0.05 and logFC >0.25.

2.6.3.1. Functional enrichment analyses. Gene Ontology (GO) is an international standardized gene functional classification system that has three ontologies: molecular function (MF), cellular component (CC), and biological process (BP). To reveal the biological function of DEPs, all peak-related genes were mapped to GO terms in the Gene Ontology database (GO.db 3.8.2(2019-04-26)), gene numbers were calculated for every term, and significantly enriched GO terms in differentially expressed genes compared to the genome background were defined by hypergeometric test.

Genes usually interact with each other to play roles in certain biological functions. Pathway-based analysis helps to further understand genes' biological functions. KEGG is the major public pathway-related database (Release 94). Pathway enrichment analysis identified significantly enriched metabolic pathways or signal transduction pathways in differentially expressed genes compared with the whole genome background.

2.6.3.2. Cell communication. We used CellPhoneDB, which contains ligand-receptor information, to analyze Expression abundance of ligand-receptor interactions between two cell types based on the expression of a receptor by one cell type and a ligand by another cell type. Based on the above analysis of the expression abundance of ligand-receptor, we obtained the number of ligand-receptor interactions between two cell types, which can make a preliminary assessment of the communication relationship between cells.

2.7. Flow cytometry

The dynamic change of main immune cells was observed by flow cytometry (FCM). Cells from bone marrow and implant surfaces were harvested as previously described and filtered through a 40 μm filter. Cells were resuspended in red blood cell lysis buffer for 5 min on ice, centrifuged, and gently washed twice with PBS. Then, the suspensions were pre-incubated with the anti-mouse CD16/32 (553140, BD Biosciences, 1 μg/mL) for 15 min on ice to block Fc receptors. After centrifuging at 550 g for 5 min at 4 °C, cell solutions were incubated with antibodies against F4/80 and CD86, CD4 and CD8, Ly6G and CD11b in the dark for 30 min at 4 °C, respectively (1 μg per 10^6 cells in 100 μL volume). All samples were centrifuged at 550g for 5 min at 4 °C and washed twice with BD wash buffer. FCM analysis was performed using a flow cytometer (CytoFLEX S, Beckman, USA) and FlowJo 10.5.0. The experiments were performed three times independently.

2.8. Neutrophil depletion

Antibodies were administered intraperitoneally according to the schedule described in Fig. S8b. The rat anti-mouse Ly6G (BE0075-1, BioX cell) antibody was administered at 200 μg per mouse two days before implantation, and every other day at 100 μg per mouse. The rat IgG2a (BE0089, BioX cell) antibody was injected as a control. Neutrophil depletion was confirmed in bone marrow by FCM (Fig. S8c).

2.8.1. μCT analysis

At designated time points, the tibiae were harvested and fixed by 4% PFA. Analysis was performed using a high-resolution μCT scanner (MILabs, U-CT-XUHR, Netherlands). The resolution was set to 10 μm per pixel. Data reconstruction was completed using Milabs Rec software, and data analysis was accomplished using Imalytics Preclinical software. Bone volume fraction (BV/TV) and trabecular thickness (Tb. Th) were measured via μCT data.

2.8.2. Immunohistochemistry

See 2.5. for detailed experimental procedures.

2.9. Cell culture

2.9.1. Neutrophil isolation

Male C57BL/6 mice aged 6–8 weeks were used and euthanized by cervical dislocation. The whole bone marrow of femurs and tibiae was isolated by flushing the intramedullary cavity with RPMI 1640 (Hyclone), supplemented with 10% fetal bovine serum (FBS, Bovogen)

and 100 U/mL of penicillin and streptomycin (p/s). The dissociated cells were filtered by a 40 μm filter, and erythrocytes were removed using a red blood cell lysing buffer. Then, neutrophils were isolated from the remaining cells by centrifugation using Histopaque 1077 and 1119 (Sigma-Aldrich, St Louis, MO). The isolated cells were resuspended for further experiments.

2.9.2. BMSCs isolation

BMSCs were obtained from the femora of 4-week-old male Sprague-Dawley (SD) rats. Bone marrow was flushed out and suspended in alpha-modified eagle medium (α-MEM, Hyclone) supplemented with 10% FBS and 100 U/mL p/s. The cells were incubated at 37 °C in a 95% humidified atmosphere with 5% CO_2. Passages three to five were used in the following experiments.

2.9.3. Elisa

After 24 h of neutrophils cultured on implant surfaces, the extracts were collected and stored at −80 °C and were subsequently analyzed by using the commercially available CXCL12 (SDF-1α) ELISA kit (BIO00002, Raybiotech) to detect the secretion of CXCL12. The protein level of CXCL12 was calculated using the absorbance value of standard samples.

2.9.4. Transwell assay

Transwell assay was conducted in the 24-well transwell chambers of 8 μm nitrocellulose pore filters (Corning-Costar, Kennebunk, USA). A density of about 5×10^4 of BMSCs was added in the upper chambers at a total of 200 μL DMEM with or without CXCR3 receptor antagonist (SCH546738, Gibco), then 500 μL different neutrophil extracts were respectively loaded in the lower chamber. Following incubation for 24 h, the cells that penetrated the membranes of the upper chambers were fixed with 4% PFA and stained with 1% crystal violet dye solution (Saichuang Technology, Wuhan, China) and photographed by a microscope. The migration was quantified by counting the stained areas in five randomly selected fields on each transwell membrane.

2.9.5. Immunofluorescent staining

To assess the effect of neutrophil extracts from different surfaces on CXCR3 expression of BMSCs. After 24 h, BMSCs were immobilized with 4% PFA, blocked in bovine serum albumin (BSA), and then incubated with primary rabbit anti-rat CXCR3 antibody (YT5277, Immunoway, 1:250) at 4 °C overnight. Alexa Fluor 488-conjugated goat anti-rabbit secondary antibody (ab150077, Abcam, 1:1000) was used for the detection. The nuclei and F-actin were labeled with 4′,6-diamidino-2-phenylindole (DAPI) and Rhodamine-phalloidin, respectively. The cells were observed with a laser confocal scanning microscope (LCSM, Nikon A1, Japan) and semi-quantified by calculating the mean fluorescence intensity of five randomly selected fields.

2.9.6. Immunoblot analysis

BMSCs were lysed with radio-immunoprecipitation (RIPA) lysis buffer and then collected after centrifuging at 12000 rpm, 15 min at 4 °C. Protein concentrations were determined by a BCA protein assay kit (PP0009, Beyotime Biotechnology). An equal amount of protein samples was loaded onto SDS-PAGE and transferred to PVDF membrane (Millipore Corp.). After blocking with 5% BSA and were incubated with the CXCR3 antibody at 4 °C overnight. Goat anti-rabbit secondary antibody was used for the detection. The immunoreactive bands were developed using an ECL chemiluminescence reagent (AlphaEaseFC, USA) and visualized using a chemiluminescence imager (Bio-Rad, USA).

2.10. Statistical analysis

The statistical significance of *in vivo* and *in vitro* data is analyzed using GraphPad Prism 9.0 (GraphPad Software, San Diego, CA, USA). Data are presented as mean ± standard deviation (SD). For comparisons among multiple groups, one-way or two-way analysis of variance (ANOVA) was used. For comparisons between two groups, two-tailed Student's T-tests were used. $P < 0.05$ was considered statistically significant ($^*P < 0.05$, $^{**}P < 0.01$, $^{***}P < 0.001$, $^{****}P < 0.0001$).

3. Results

3.1. Evaluation of bone healing of implants with different osteogenic and immunomodulatory properties

Implant materials with different osteogenic properties were prepared including SR, SLA, PT, and SS as previously described [18]. The surface of SR presented a honeycomb structure with more dense micro/nano-sized particles and increased roughness than that of the SLA surface. SS and PT surfaces were smooth without pits (Fig. 1a, S1a). The contact angle of the freshly prepared SR surface was under 5°, indicating a superhydrophilic surface (Fig. 1b, S1b). As for the ion release, after immersing the SR implant in media, the measured release curve of Sr^{2+} in the leaching solution showed the release of Sr^{2+} gradually decreased until 21 days (Fig. 1c). Detailed physical characterizations were displayed in Fig. S1.

To evaluate the osteogenic capacity and immunomodulatory effect of different biomaterials, four types of implants were placed into the tibiae of mice, and the sham site as a control. The workflow was shown in Fig. 1d. The analysis of BIC% showed the highest osteogenic potential of SR implant, followed by SLA and PT implants, and the lowest was SS implants with little new bone formation (Fig. 1e and f). Histological sections showed inflammatory cells infiltration and fibrous connective tissue only around SS implants, with a large number of foreign body giant cells (FBGCs) adhered to SS interface and more trap-positive multinucleated cells (Fig. S2). The expression level of osteogenic-related proteins was lowest in the SS group, and was highest in SR group (Fig. 1g–j). In summary, the SR implant exhibited a rougher and superhydrophilic surface with increased new bone formation while the SS implant was surrounded by plentiful FBGCs and collagen fibers, which indicated fibrosis.

Bone tissue RNA-sequencing (RNA-seq) analysis for samples harvested 3 days ($n = 3$) after post-implantation. Sequence alignment was performed with 22298 genes of the genome (Ensembl_release100 version). Principal component analysis (PCA) revealed that the SR, SLA, and PT groups had similar gene expression profiles (Fig. 1k). GO analysis showed that the implantation of biomaterials induced the biological function associated with extracellular matrix organization, system development, multicellular organism development, etc. when compared with sham sites (Fig. S3a). SR implant induced the differentially expressed genes associated with extracellular structure organization, immune process, and skeletal system development compared with the SS group (Fig. 1l, S3b). In more detail, SR group promoted the biological functions of collagen binding, ossification, osteoblast differentiation, and bone remodeling. Nevertheless, SS group induced stronger inflammation via activating immune response-related processes (Fig. 1m). Thus, the prognosis of implants depends on the degree of difference in foreign body reactions caused by biomaterials. SR implants facilitated osteogenesis by upregulating the process of osteogenic responses and leading an appropriate immune reaction to prevent the loss of foreign body equilibrium.

3.2. scRNA-seq of peri-implant cell heterogeneity during bone healing

A response to a foreign body is initiated due to the induction of innate and non-specific defense mechanisms of the body, usually lasting from a few hours to four days and having a continuous effect on biomaterial integration [19]. To decipher the microenvironment of bone substitution materials, we performed scRNA-seq on unsorted cells around SS, PT, SLA, and SR implants and in the SHAM site three days post-implantation (Fig. 2a).

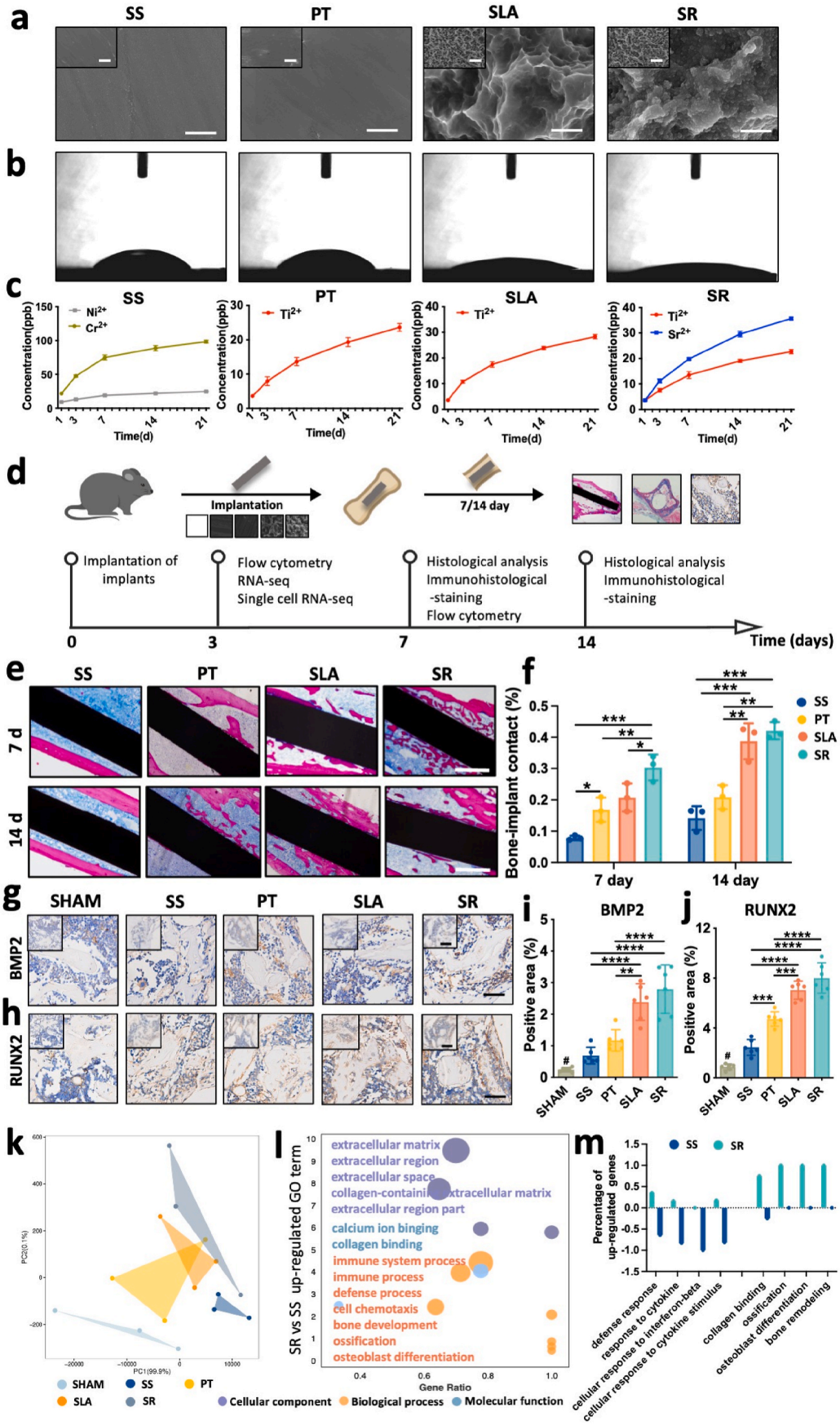

Fig. 1. Evaluation of the osseointegration and immunomodulatory property of murine tibiae implanted with four types of implants.
a Surface morphology of SS, PT, SLA, SR surfaces. Scale bar: 500 nm b Representative images of hydrophilicity measurement of the SS, PT, SLA, SR surfaces. c Cumulative release profile of Ni^{2+}, Cr^{2+}, Ti^{2+}, and Sr^{2+} ions from SS, PT, SLA and SR implants after incubation for 21 days. d Workflow of evaluating bone healing of different implants in murine tibiae. e Histological images of the implants (black) and peri-implant bone (pink) formed at 7 and 14 days after implantation. Scale bar: 500 μm f Quantitative analysis of bone-implant contact rate (BIC%). g,h Immunohistochemistry staining of osteogenic-related proteins BMP2 and RUNX2 (brown) after 14 days post-implantation. Scale bar: 100 μm; 250 μm (insert). i,j Semiquantitative analysis of the immunohistochemistry staining of BMP2 and RUNX2. k Principal component analysis (PCA) plot showing the distribution of differentially expressed genes (DEGs) of the bone marrow of the SHAM, SS, PT, SLA, and SR groups ($n = 3$). l Gene ontology (GO) analysis showing the differentially expressed gene sets enriched in GO term of SR group compared with the SS group. Circle size denotes the gene number in each GO term. m The up-regulated genes of SR group were enriched in osteogenesis-related biological processes, while the immune response-related functions were enhanced in the SS group.

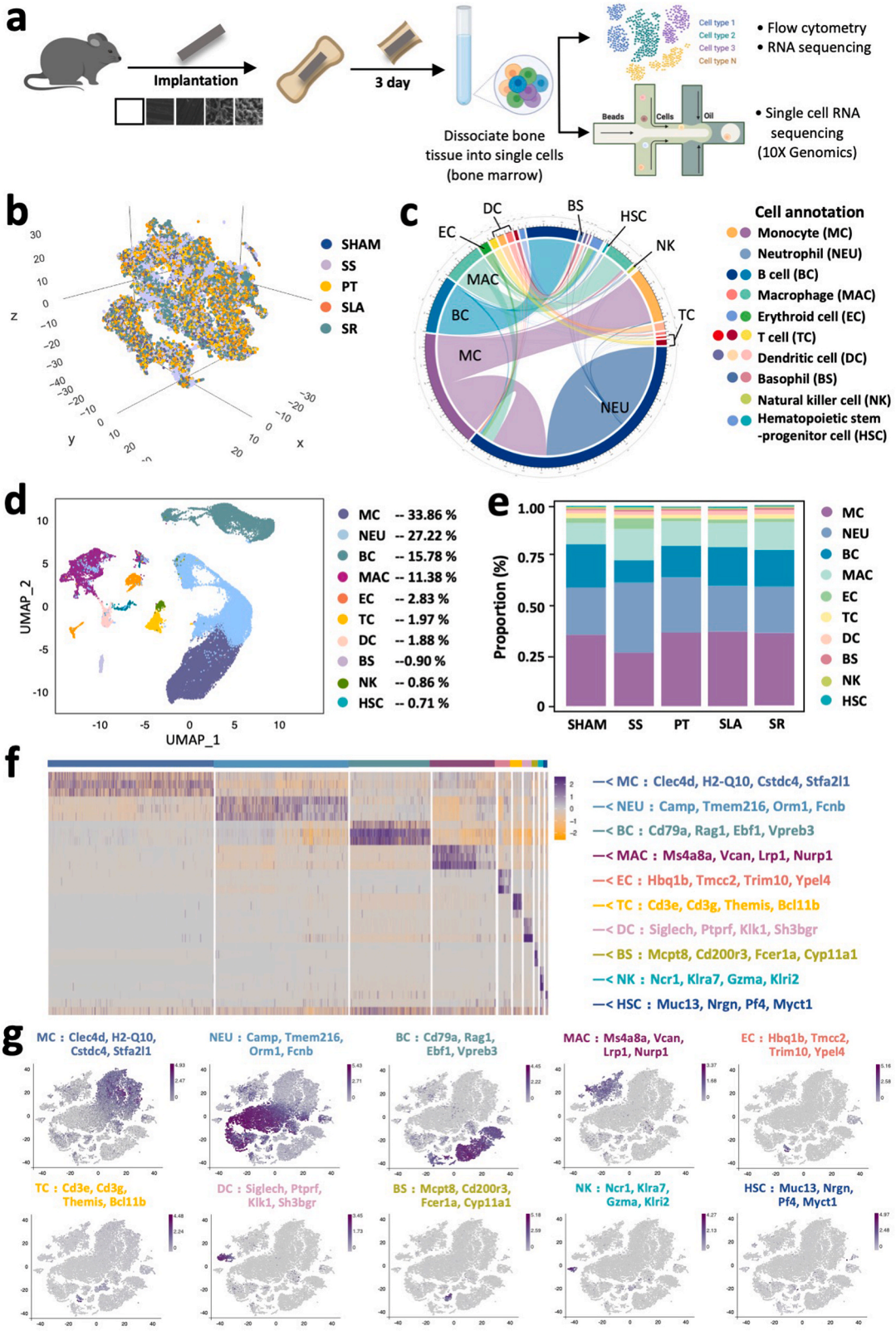

Fig. 2. Overview of cell heterogeneity in bone marrow three days after implantation by scRNA-seq.
a Schematic flow of bone marrow cell collection, cell isolation, capture by droplet-based device, and sequencing. b Three-dimensional scatter diagram visualizing epigenomic profiles at the sample level. c Circle diagram displaying the unsupervised hierarchical cell clusters. In total, 40043 single-cell transcriptomes were collected and classified into 10 cell types. d UMAP plot revealing cell heterogeneity with 10 distinct clusters after cells annotation. General identity and proportion of each cell cluster is defined on the right. e Bar plot showing the proportion of each cell cluster among five groups. f Heatmap of differentially expressed genes. Selected genes for each cluster were color-coded and shown on the right. g Feature plots of expression distribution for cluster-specific genes. Expressed cells were color-coded and overlaid onto the t-SNE plots. Unexpressed cells were colored gray.

After standard data quality control and filtering (Fig. S4a), a total of 40043 cells were captured, including 7970 cells from the SHAM group, 13061 cells from SS group, 9325 cells from PT group, 6206 cells from SLA group, and 12203 cells from SR group (Table. S2). Based on the analysis of cell clusters classification, the t-SNE nonlinear clustering method was further used to visualize the classification results of single-cell subclusters (Fig. 2b, S4b, S4c). Unbiased clustering of the cells assigned to ten main clusters based on SingleR identification. Each cluster was identified via cell annotation (Fig. 2c, S4d): (1) monocytes (MC), (2) neutrophils (NEU), (3) macrophages (MAC), (4) B cells (BC), (5) T cells (TC), (6) dendritic cells (DC), (7) Erythroid cells (EC), (8) Basophils (BS), (9) Natural killer cells (NK), and (10) Hematopoietic stem progenitor cells (HSC) (Fig. 2d). The proportion of cell clusters among five groups was shown in the bar chart (Fig. 2e) and detailed data were listed in Table. S3. It exhibited an obvious increase in the proportion of neutrophils in SS group (35.02%) compared with SHAM

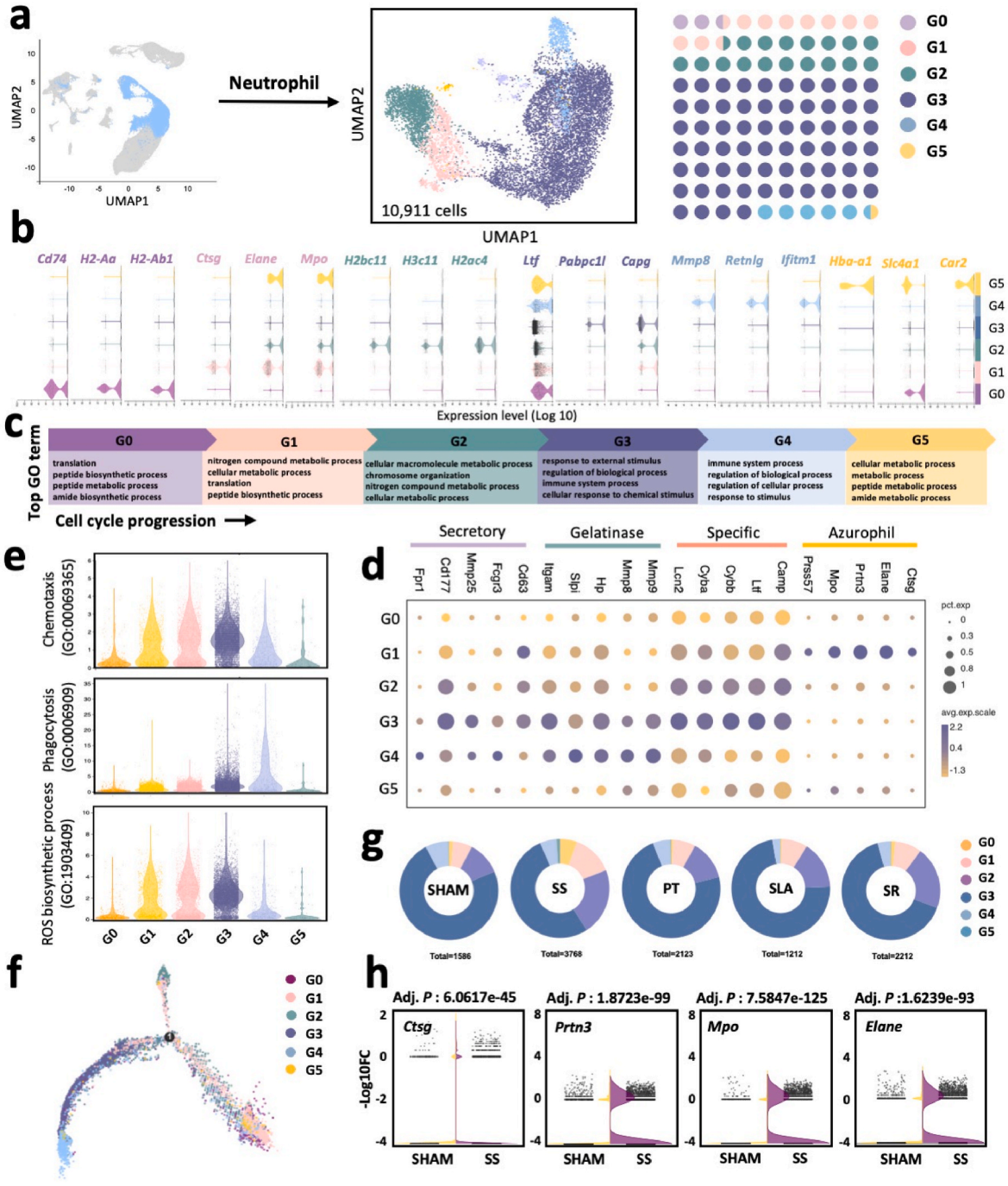

Fig. 3. Transcriptomic analysis reveals distinct expression signatures during neutrophil development.
a Subclustering of neutrophils further identified six distinct subclusters. Color-coded UMAP plot showing the definition of each neutrophil subcluster. b Violin plot of differentially expressed marker genes for six neutrophil subclusters. c Enriched gene sets in GO analysis for each neutrophil subcluster. d Expression of genes encoding granule production, assessed in neutrophil subclusters. e Violin plot of chemotaxis (GO:00069365), phagocytosis (GO:0006909), and ROS biosynthetic process (GO: 1903409) scores for subclusters. f Pseudo-temporal ordering of neutrophil subclusters along the trajectory with the distinctly differentiated cell subcluster. Different colors represent different subclusters. g Circle diagrams depicting the percentage of each neutrophil subcluster in the SHAM, SS, PT, SLA, and SR groups. h Gene pod plot showing the different expression levels between SS and SHAM groups.

group (23.57%), and there were similarities among other implant materials (min: 22.91%; max: 27.60%), which may indicate titanium-based implants do not induce neutrophil overreactions. The proportion of macrophages in SS group (15.53%) also slightly increased compared with other groups (min: 10.15%; max: 13.88%). On the contrary, there was a significant decrease in the proportion of monocytes and B cells in the SS group (MC: 26.72%; BC: 11.13%) compared with other groups. Of note, the proportion of erythroid cells increased in SS group (5.35%) compared with SHAM group (2.47%), whereas the opposite decreased trend in other implant materials (min: 1.53%; max: 1.93%). Although the trauma caused by the implantation was the same, the subsequent platelet activation and coagulation reaction degree were different due to the difference in the material's hemocompatibility. Differentially expressed marker genes were shown in the form of a heatmap (Fig. 2f), t-SNE plots (Fig. 2g), and a Table. S4.

3.3. SR implants were accompanied by more mature G3 and G4 neutrophils in the biomaterial-based osteoimmune microenvironment

To dissect neutrophil heterogeneity, unsupervised clustering was used and neutrophils were clustered into six subclusters, G0 through G5, according to the phase of cell cycle (Fig. 3a and b) [20–22]. G0 neutrophils typically expressed *Cd74*, *H2-Aa* and *H2-Ab1* and are granulocyte monocyte progenitor (GMP) cells. G1 neutrophils highly expressed *Ctsg*, *Elane*, and *Mpo*, presented in azurophil granules that were crucial in antimicrobial oxidizing, and correspond to neutrophil progenitor cells (proNeu). G2 neutrophils specifically expressed *H2bc11*, *H3c11*, and *H2ac4* and are neutrophil precursor cells (preNeu). Further combination with GO analysis indicated that G1 to G2 subclusters underwent active proliferation and cell division (Fig. 3c). Cell cycle-related genes including *Mki67*, *Cdk1*, and *Top2a* were more highly expressed in earlier phases of neutrophil maturation (G0, G1, and G2), during cells progress from GMPs to mNeu (Fig. S5a). The expression of azurophil, specific, gelatinase, and secondary granular genes was examined in neutrophil subclusters to help us judge the differentiation and function of neutrophils (Fig. 3d). And neutrophils in earlier phases participated in defense response, enzymatic hydrolysis, and inflammation-related pathways (Fig. S5b). G3 cells followed G2 expansion and began to exert an immunomodulatory ability with high expression of *Ltf*, *Pabpc1l,* and *Capg* [22,23]. As the most mature neutrophils (mNeu), G4 cells highly expressed *Mmp8*, *Retnlg*, and *Ifitm1* and played a major immunomodulatory role [22]. The key genes enriched in chemotaxis, phagocytosis, and ROS production were highly expressed among G3 and G4 (Fig. 3e, S5c). Neutrophils have a short lifespan, starting from G0 cells in BM and ultimately ending up with G5 cells in peripheral tissues, with high expression of *Hba-a1*, *Slc4a1*, and *Car2* (Fig. 3f) [24,25].

Notably, neutrophils were the most abundant cells surrounding the SS group, and the proportion of G1 cells in SS group (13.40%) was almost twice that of other groups (min: 6.37%; max: 8.77%) (Fig. 3g), combining with the transcriptional level of proteinases was increased in SS group. The above evidence suggested that the SS implant elicited more inflammatory neutrophils extravasation and overshooting inflammatory response (Fig. 3h). It was also noted that the proportion of G3 and G4 cells was significantly higher in SR group (69.25%) than that of SS group (57.99%), which was associated with the ability of mature neutrophils to phagocytose pathogens and recruit more cells to improve tissue repair. Thus, the biomaterial affects the differentiation process and functional status of neutrophils. SS group had the most neutrophil recruitment and the highest proportion of immature G1 cells, while SR group was surrounded by more mature G3 and G4 cells, and different phages of neutrophils play their respective roles in shaping the osteoimmune microenvironment.

3.4. Distinct macrophage phenotypes regulate bone tissue regeneration

After implantation, macrophages were recruited at the early stage of injury and differentiated into different types. Increasing evidence showed that diverse phenotypes of macrophages play indispensable roles in tissue repair, fibrosis, and regeneration [26]. Unsupervised analysis of gene-expression profiling identified five subclusters of macrophages (Fig. 4a). Macrophage subclusters were named S100a8^{hi}, FcgR1^{hi}, Il1β^{hi}, H2-Aa^{hi}, and C1qa^{hi} according to their highly expressed genes (Fig. 4b) [27,28].

Traditionally, the role of macrophages in tissue regeneration is always accompanied by their polarization [29,30]. Conventional M1/M2 typing was not completely consistent with the subclusters in this study. Il1β^{hi} subcluster highly expressed inflammatory genes that were enriched in defense response and osteoclast differentiation, performing similar functions as pro-inflammatory macrophages (M1) (Fig. 4c, S5d) [31,32]. H2-Aa^{hi} and C1qa^{hi} subclusters tend to be like anti-inflammatory macrophages (M2) with a higher transcriptional level of tissue repair and inflammation resolving-related genes (Fig. 4c) [29,33,34]. KEGG pathways of H2-Aa^{hi} subcluster enriched in regulating Th1/2 and Th17 cell differentiation and C1qa^{hi} subcluster were involved in activating leukocytes and producing cytokines. S100a8^{hi} and FcgR1^{hi} subclusters did not conform to the phenotypic classification. S100a8^{hi} subcluster played a role in the spliceosome and oxidative phosphorylation pathway, while FcgR1^{hi} subcluster participated in the NOD-like receptor signaling pathway and osteoclast differentiation (Fig. S5d).

It was shown that the SS group had the highest proportion of S100a8^{hi} subcluster (57.8%) than other groups (min: 25.84%; max: 33.66%) (Fig. 4d). Conversely, an obvious increase in the proportion of FcgR1^{hi} subcluster among titanium-based groups (min: 45.65%; max: 51.83%) when compared with SS group (25.37%). Also, the proportion of Il1β^{hi}, H2-Aa^{hi}, and C1qa^{hi} in titanium-based groups (min:20.11%; max:22.33%) and SHAM group (22.00%) slightly increased, while SS group (16.82%) was lower. To further explore the continuum of phenotype switching in macrophage subclusters, the differentiation trajectory analysis was carried out. S100a8^{hi} subcluster was broadly distributed at the start of the pseudo-time path on the left side of trajectory, while FcgR1^{hi} subcluster was dominantly gathered at the terminal trajectory (Fig. 4e). Functional heterogeneity among individual subclusters was further investigated, S100a8^{hi} subcluster demonstrated essentially enriched in oxidative phosphorylation, IL-17 signaling pathway, and necroptosis. Meanwhile, the expression of related genes was increased in SS group compared to other groups (Fig. 4f). Genes involved in immunomodulatory functions, including chemokine signaling pathway, phagosome, and antigen process and presentation were activated in FcgR1^{hi} subcluster, which showed the lowest level in SS group (Fig. 4g).

In brief, SS group with more S100a8^{hi} subcluster was considered an early responder to initiate and amplify the inflammatory response in the acute stage of implantation. Instead, titanium-based groups promoted macrophages to differentiate into FcgR1^{hi} subcluster and were accompanied by more differentiated macrophages that played an immunoregulatory role in alleviating inflammation and facilitating bone regeneration.

3.5. Monocytes and dendritic cells accelerated differentiation processes after implantation

In the titanium-based implants, monocytes were the largest cell cluster (min: 36.22%; max: 37.37%) and distinguished into two subclusters based on their expression of *Ly6c* and *Ccr2*. The Ly6C^{+} CCR2^{hi} and Ly6C^{-}CCR2^{low} subclusters were equivalent to human classical/intermediate monocytes and non-classical monocytes, respectively (Fig. 5a and b) [35]. Under homeostasis, monocyte subclusters represented stages in a developmental sequence, with classical monocytes first differentiating into intermediate monocytes and then transforming into non-classical monocytes under Notch2 signaling [36,37]. After implantation, classical/intermediate monocytes (mean: 90.29%) were rapidly recruited to the implant site and exerted the immune regulation

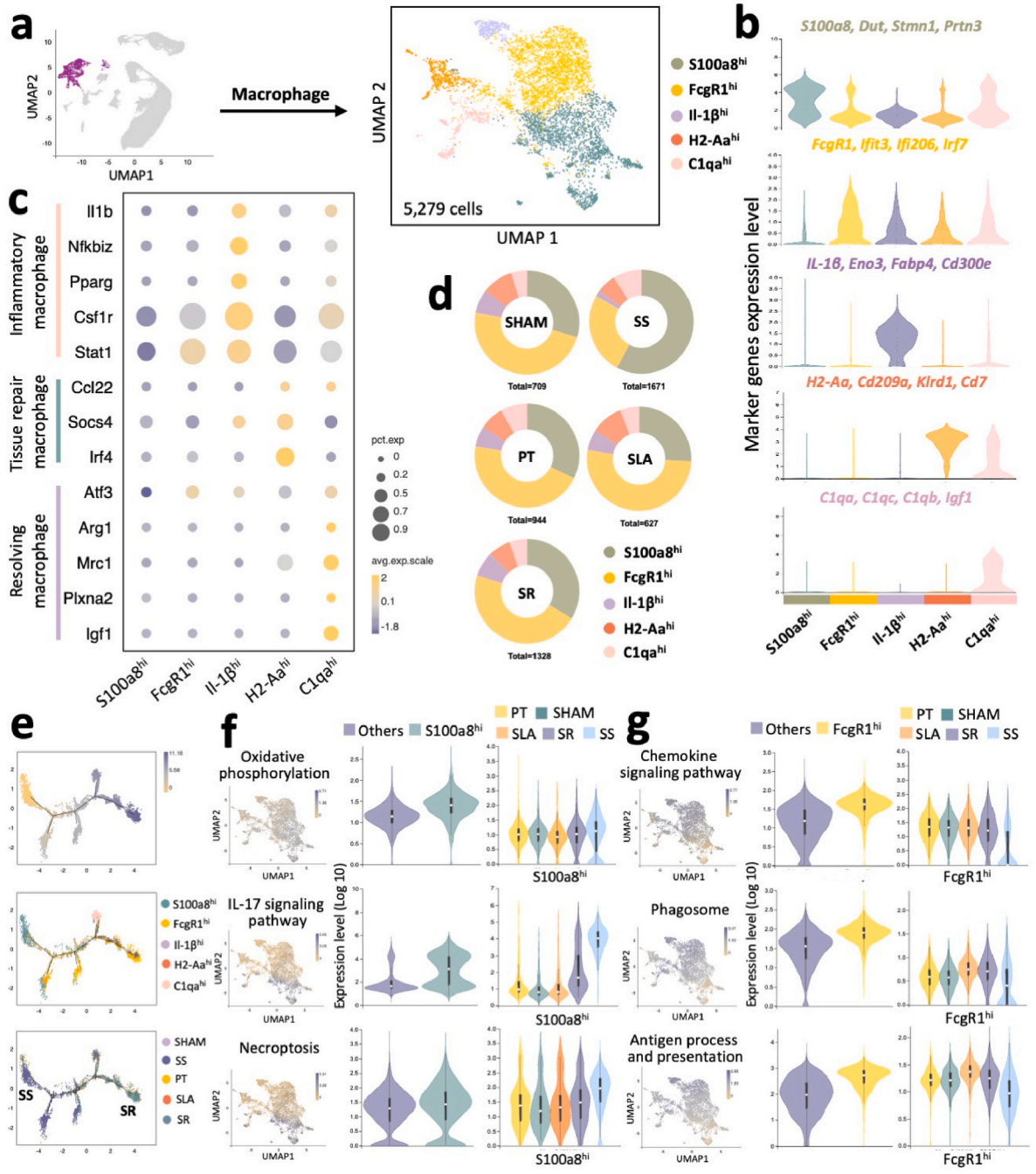

Fig. 4. Subclustering of macrophages reveals cell heterogeneity induced by implant materials.
a Subclustering of macrophages further identified five distinct subclusters. Visualized UMAP plot of macrophages is shown color-coded. b Violin plots of distinct phenotypic signatures for each macrophage subcluster. c Expression of canonical phenotype marker genes of inflammatory, tissue repair, and resolving macrophages. d Circle diagrams depicting the proportion of each macrophage subcluster in the SHAM, SS, PT, SLA, and SR groups. e Pseudo-temporal ordering of macrophages and the definition of subcluster along the trajectory with the pseudo-time information (up), distinctly differentiated subcluster (middle), and sample information (down), respectively. f,g Up-regulated genes in the IL-17 signaling pathway, oxidative phosphorylation, necroptosis, chemokine signaling pathway, phagosome, antigen process and presentation among macrophages, each point is depicted as a single cell. Cells with indicated signaling activation were colored in shades of purple-red, and those without signaling activation were colored in yellow. Boxplots between the targeted macrophages subcluster and the remaining four subclusters were shown on the right, the lists of genes used to compute enrichment are according to KEGG: ko00190 (oxidative phosphorylation), ko04657 (IL-17signaling pathway), ko04217 (necroptosis), ko04062 (chemokine signaling pathway), ko04145 (phagosome), ko04612 (antigen process and presentation).

effect such as defense response, immune system process, and response to external stimulus (Fig. 5c). Then, a small number of non-classical monocytes (mean: 9.71%) displayed a patrolling behavior to regulate metabolism and release cytokines [38].

KEGG analysis showed that the heterogeneity of monocyte clusters was closely related to the osteoclast differentiation pathway (Fig. 5d). Classical/intermediate monocytes up-regulated the osteoclastogenesis-related genes (*Csf1, Fos, Nfatc1, Mmp9*), while non-classical monocytes up-regulated some key factors (*Cd47, Cd14, Il4*) associated with FBGCs formation (Fig. 5b) [39]. The SR group had the lowest proportion of classical/intermediate mononuclear cells (78.79%) and the least TRAP-positive multinucleated cells (Fig. S2c). Meanwhile, it was

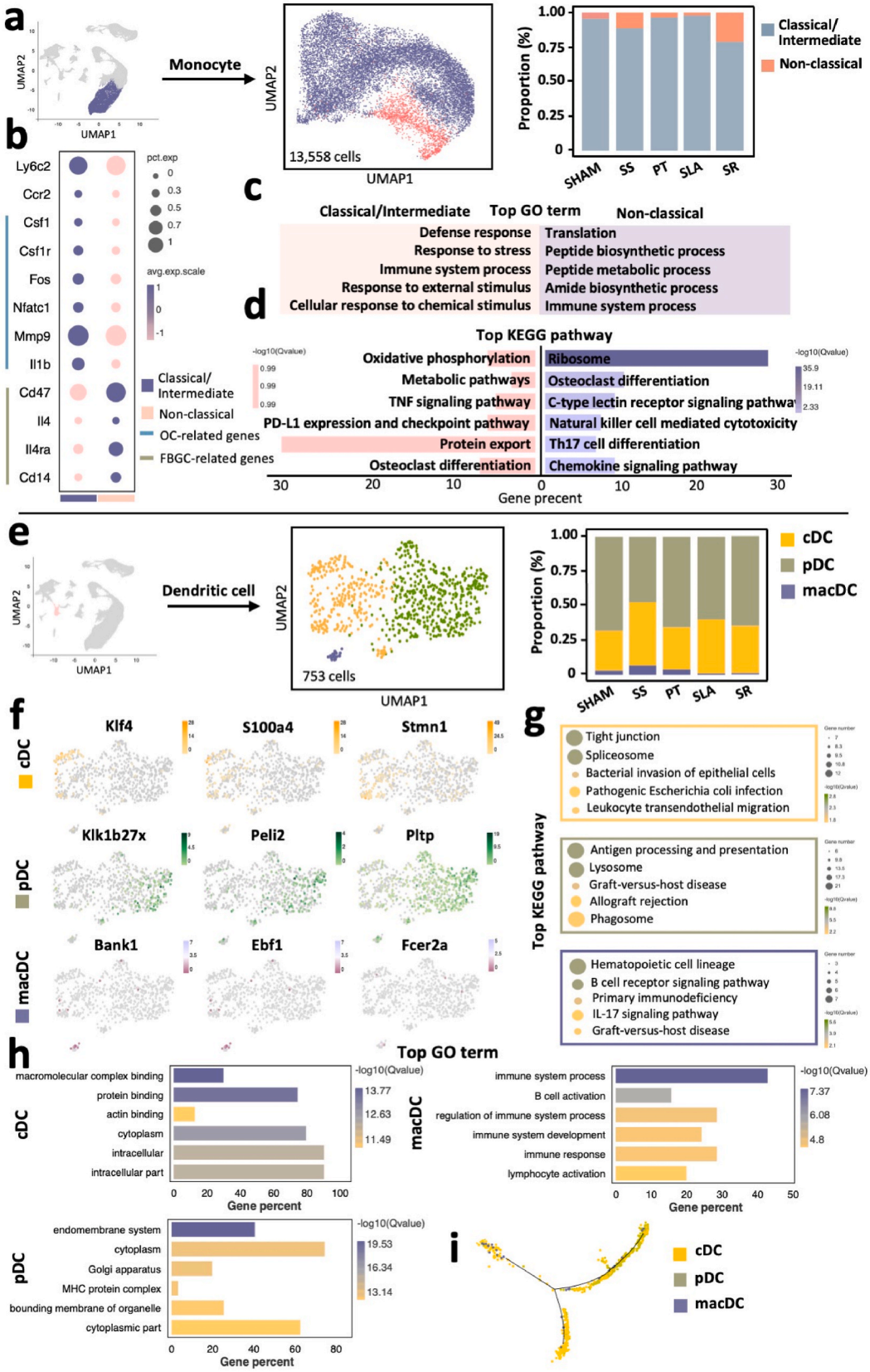

Fig. 5. Monocytes and DCs accelerated the differentiation process after implantation.
a Subclustering of monocytes further identified two distinct subclusters. Color-coded UMAP plot was shown and each monocyte subcluster was defined on the right. b Dot plot of specially expressed genes for monocyte subclusters. c, d Enriched gene sets of classical/intermediate and non-classical monocytes in top GO term (c) and top KEGG pathway (d). e Subclustering of DCs further identified three distinct subclusters with visualized UMAP plot. f Feature plots depicting single cell expression of identified genes in DCs. g Enriched gene sets of DCs in top KEGG pathway. h Top GO terms of DC subclusters. i Pseudo-temporal ordering of three subclusters of DCs along the trajectory.

noteworthy that the proportion of non-classical monocytes in SS group (11.41%) was significantly higher than that in PT group (3.59%), which was consistent with the number of FBGCs on the interface of implants. The above evidences suggested that monocyte subclusters were closely related to the differentiation of the two kinds of multinucleated cells and influenced by biomaterial properties.

DCs are a diverse group of specialized antigen-presenting cells with key roles in the initiation and regulation of innate and adaptive immune responses [40]. Recently, some studies reported that titanium-based implants with different surfaces could induce DCs into different immune states, influencing the early immune responses around implants and subsequent osteogenesis [41–43]. In this study, DCs were classified into three subpopulations (Fig. 5e) [44]. Those characterized by increased expression of *Klf4*, *S100a4*, *and Stmn1* genes were named conventional DCs (cDCs). Another subcluster characterized by an elevated transcriptional level of *Klk1b27x*, *Peli2*, and *Pltp* was assigned plasmacytoid DCs (pDCs) (Fig. 5f). According to the results of KEGG analysis (Fig. 5g), pDCs primarily played the function of antigen processing and presentation. And further analysis found that the highly expressed histocompatibility complex (MHC) molecules of pDCs are mainly related to positive regulation of antigen presentation and T cell-mediated cytotoxicity (*Cd74*, *B2m*, *H2-k1*, and *H2-d1*) (Fig. S6a). The remaining subcluster with the least proportion resembled macrophages under inflammatory conditions, which were defined as macrophage-like DCs (macDC), with a high expression of *Bank1*, *Ebf1*, and *Fcer2a* [43,45,46]. MacDCs effectively initiated leukocyte and lymphocyte activations and immune-related processes [47,48], which was consistent with our finding that macDCs highly expressed genes of B cell activation and IL-17 signaling pathway (Fig. 5h, S6b, S6c). The pseudo-time analysis revealed two terminally differentiated clusters (cDCs and macDCs) stemming from precursor cells (Fig. 5i, S6d). Notably, the proportion of macDCs increased in SS group (6.67%) compared with SHAM group (3.00%), whereas an opposite decreasing trend in SLA (0.93%) and SR (0.95%) groups, which may indicate that titanium-based implants created a relatively gentle immune environment, avoiding overzealous inflammatory responses.

3.6. Bone marrow is where B and T lymphocytes development takes place

B cells differentiate from HSCs in a highly coordinated but flexible pathway. Prominent transcriptional factors, including *Tcf3, Ebf1, Foxo1, Pax*5, and *Ikzf1*, orchestrated the fate of B-cell and directed the development of HSCs into common lymphoid progenitors (CLPs) (Fig. S6e) [49]. CLPs then differentiated into progenitor BC (proBC) (*Mmrn1, Arpp21, Vpreb2*) and precursor BC (preBC) (*Rag1, Il2ra, Ael5c*) (Fig. 6a and b) [50]. After assembling with the pre-B cell receptor (BCR), they became immature B cells (imBs) (*Aspm, Ccnb2, Ccnb1*) [51,52]. ImBs migrated out of bone marrow, becoming transitional B cells (TBs) (*Hck, Srpk3, Pld4*) and entering peripheral lymphoid organs. After reaching the spleen and developing into follicular B cells (FOBs) (*Fcel5, Nid1, Atxn1*), they regained circulation ability and arrived at the immunoreaction site to play a role in the immune system regulation, T cell activation, and biological process (Fig. 6c and d) [53]. Under the stimulation of implantation, re-recruited B cells differentiated into naïve B cells (NBs) (*Pgap1, Gpr174, Gimap3*) and terminally matured into immunoglobulin-secreting plasma B cells (PBs) (*E2f8, Rrm2, Esco2*) (Fig. 6e), which rapidly proliferated and produced high affinitive antibodies to destroy pathogens [54]. In our study, there was no significant difference among B cell subclusters in different implant materials except PBs. The proportion of PBs was increased in SS group (25.71%) compared with other groups (mean: 11.42%), especially SHAM group (8.04%), which may indicate that SS group caused a strong humoral immune response.

The time of detection was 3 days after implantation, and only a few T cells were captured in the acute inflammatory response stage. Within the T cell clusters, which were differentiated by CLPs in the bone marrow and expressed specific genes (*Cd3e*, *Cd3d*, etc.) and were identified as γδ T, regulatory $CD4^+$ T ($CD4^+$ Treg), Naïve $CD8^+$ T, tissue-resident memory $CD8^+$ T ($CD8^+$ Trm), and mitotic T cells (Fig. 6f, S6f) [50]. Among them (Fig. 6g), γδ T cells were defined according to the expression of *Qrfp, Klra7, Spry*, and *Cd244a*, and were identified as a primary initiator of leukocyte and lymphocyte activation and IFN-γ production, which promoted the bone formation and facilitates bone fracture healing [55,56]. The main transcription factors that regulated $CD4^+$ Treg cells development were *Cd4* and *Foxp3* (Fig. S6g) [57]. $CD4^+$ Treg cells regulated immune tolerance and immune process, which produced IL-10 and TGF-β to remodel bone formation [58,59]. $CD8^+$ T cells were characterized by expressed *Cd8a*, then, Naïve $CD8^+$ T cells and $CD8^+$ Trm cells were distinguished by the expression of *Igfbp4, Dapl1, Ccr7, Cd8b1*, and *Ifit1, Isg15, Ifit3, Gbp2*, respectively. $CD8^+$ Trm cells were mainly involved in regulating the defense process, and they can secrete OPG, IFN-γ, and TNF-α which have dual effects on osteogenesis [60,61]. Combined with GO analysis (Fig. 6h), the biological process of mitotic T cells with high expression of *Gda, Pclaf, Mmp8,* and *Ltf* was correlated with the metabolic process. And mitotic T cells were located at the beginning of the pseudo-temporal ordering, indicating that they differentiated further under a highly ordered process (Fig. 6i) [62].

3.7. Cell communication reveals the potential interactions between hematopoietic stem cells and neutrophils

Bone regeneration relies on the coordination of cellular activities, which depend on cell-cell interactions across diverse cell types. Thus, elucidating the potential communications in the osteoimmune microenvironment will shed light on the mechanisms of FBR equilibrium and bone homeostasis after implantation. We used CellPhoneDB to analyze the cross-talk and possible mutual effects of different cell types [63]. Heatmap and the chord diagram showed the interactions and the number of ligand-receptor pairs between two cell types (Fig. 7a and b), suggesting that the communication among cells was complicated. Of these, the interactions between neutrophils, macrophages, B cells, and HSCs appeared to be the strongest.

Among the major cell clusters, HSCs had multipotentials because of their ability to self-renewal and produce daughter cells [64]. HSCs exist in the bone marrow and interact with cells that secrete or express cytokines and growth factors to facilitate their growth and differentiation [65]. It was demonstrated that the high expression of osteogenic genes in HSCs, indicated that they may further differentiate into osteogenic progenitors (Fig. S7a). Interactive plots for single-cell clusters hinted that HSCs interacted most strongly with neutrophils and macrophages (Fig. S7b). Then, the ligand-receptor pairs between immunocytes and HSCs were next explored. In brief, the top 25 ligand-receptor pairs acted on cell growth, cell adhesion/migration, proliferation/apoptosis, and angiogenesis. etc (Fig. S7c). In combination with the dynamic changes of main immunocyte types with time, neutrophils were the most abundant cells in the early stage and peaked at 3 days (Fig. S8a). Thus, the top 25 ligand-receptor pairs between neutrophils and HSCs were further analyzed, which mainly acted on cell growth, G-protein coupled receptors, stromal cell chemotaxis and angiogenesis, etc (Fig. S7d). Among them, CXCL12 is known to play an important role in MSC migration and osteogenesis which deserved further study (Fig. 7c) [66].

3.8. Neutrophils play a promotive role in bone regenerative process and osseointegration

Neutrophils have pro-vascularization potential and can orchestrate tissue repair and ectopic bone formation [67,68]. We further assessed the correlation between the number of neutrophil clusters and the number of HSCs around implants *in vivo*. Among the five groups, both the number of G3 neutrophils and G4 neutrophils had a positive relationship with the number of HSCs (Fig. S7b). However, the role of

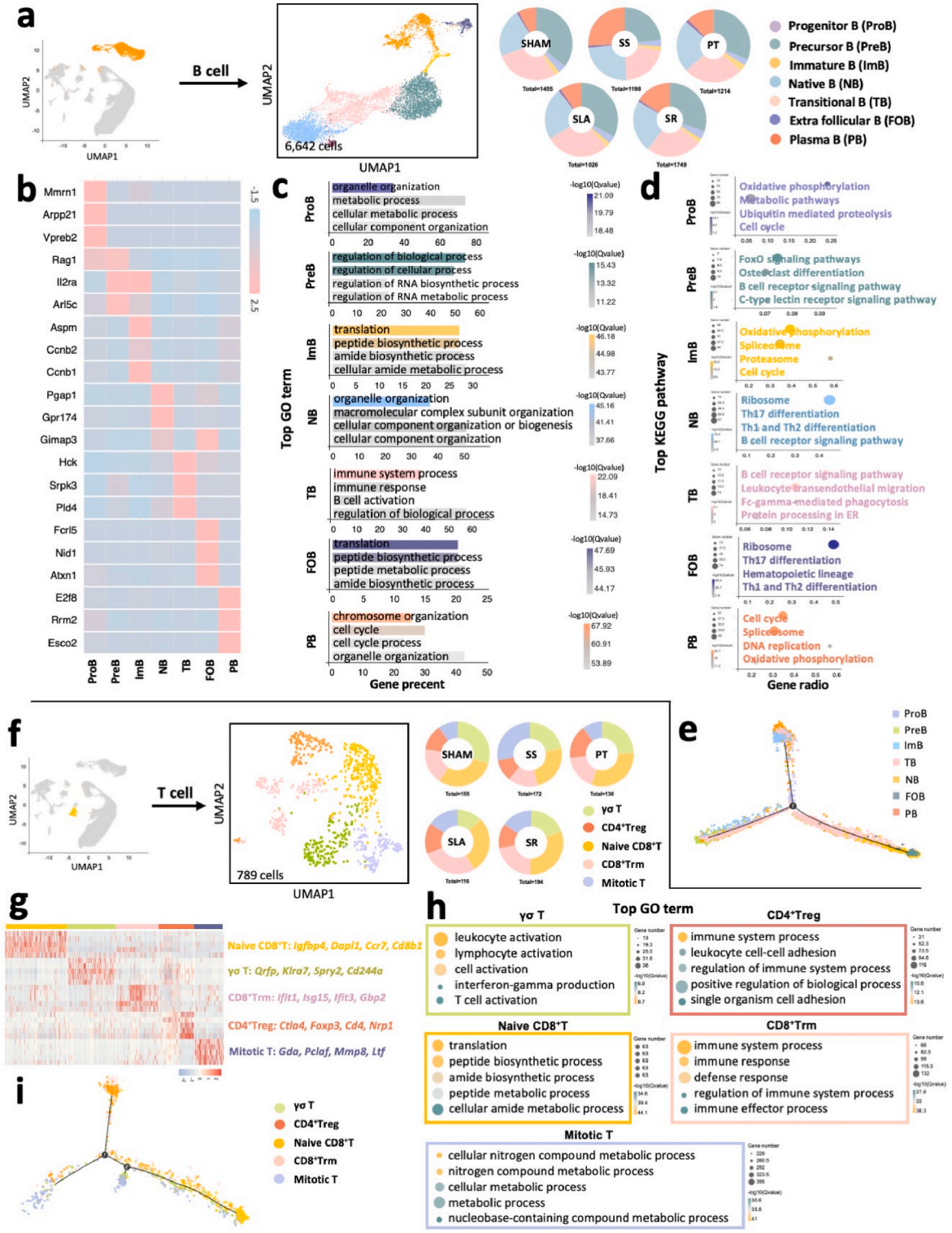

Fig. 6. B and T lymphocytes harbor various distinct types.
a Visualized UMAP plot of B cell subclusters and circle diagrams depicting the component of B cell subclusters in the SHAM, SS, PT, SLA, and SR groups. b Heatmap of marker genes transcription for each B subcluster. c,d Enriched gene sets of B cell subclusters in GO analysis (c) and KEGG pathway (d). e Pseudo-temporal ordering of seven B cell subclusters along the trajectory. f Visualized UMAP plot of T cell subclusters with circle diagrams depicting the composition of T cell subclusters. g Heatmap of marker gene transcription for each T subcluster. h GO enrichment analysis of the biological functions of each T subcluster. i Pseudo-temporal ordering of five T cell subclusters along the trajectory.

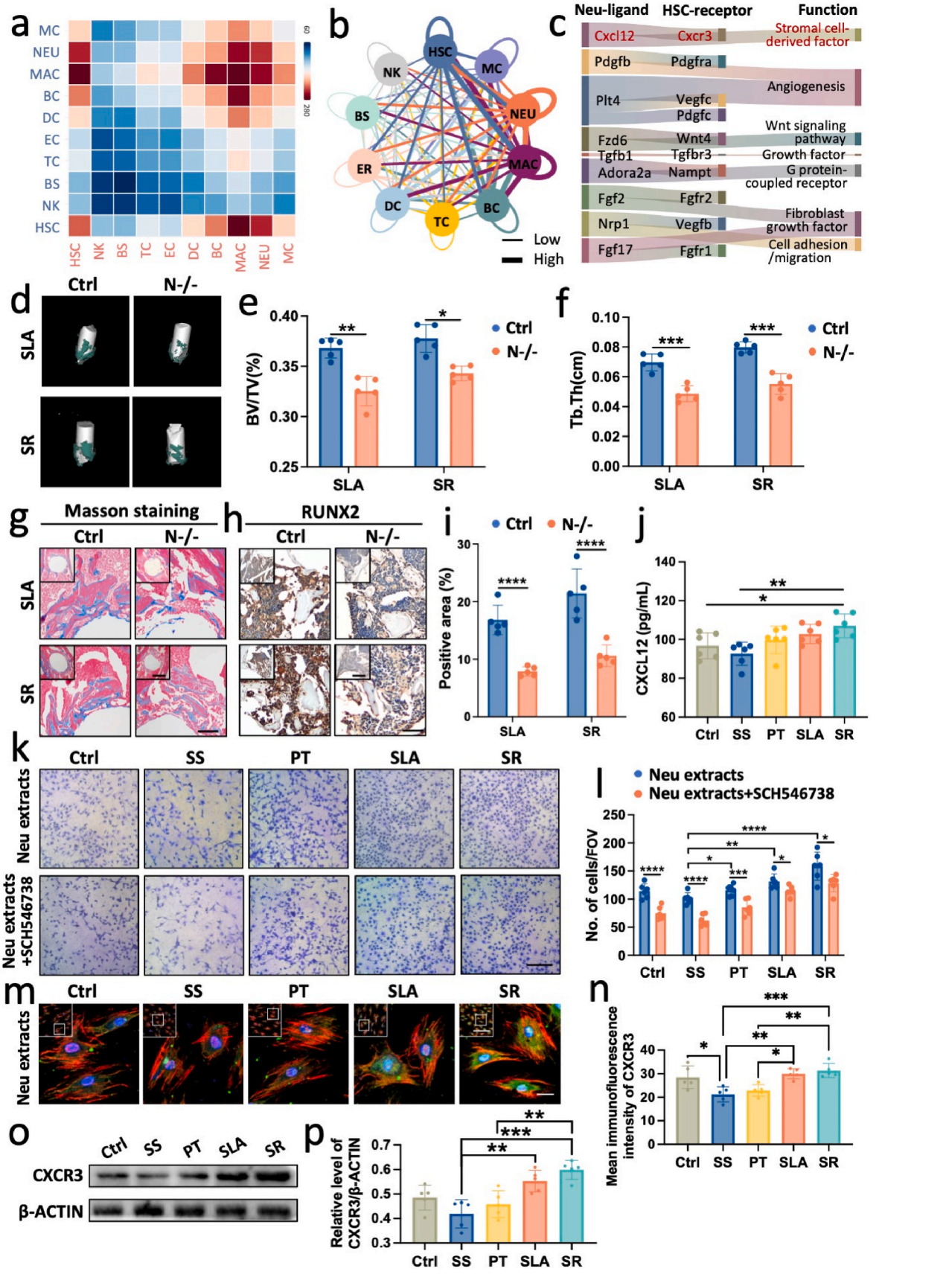

(caption on next page)

Fig. 7. Cell-cell interaction analysis builds a bridge between neutrophils and hematopoietic stem cells and neutrophils play a promotive role in osseointegration. a Heatmap showing the number of interactions among ten cell clusters. b Chord diagram of cellular communication relationship among ten cell clusters. Networks depicting cell types as nodes and interactions as edges. Edge thickness is proportional to the number of interactions between the connecting types. c Chord diagram visualizing the top 10 ligand-receptor pairs between neutrophils and HSCs. d Three-dimensional reconstruction images of the bone formation after implantation *in vivo,* green volumes represented bone tissue. e, f Analysis of BV/TV (e), Tb.Th (f) in each group. $^{*}P < 0.05$, $^{**}P < 0.01$, $^{***}P < 0.001$ compared with the Ctrl group ($n = 5$). BV/TV, bone volume/total volume; Tb.Th, trabecular thickness. g Representative images of Masson staining showing the bone regeneration after implantation. Scale bar: 250 μm; 750 μm (insert). h Immunohistochemistry staining of RUNX2 (brown) at the implantation site after 14 days. Scale bar: 100 μm; 250 μm (insert). i Semiquantitative analysis of the immunohistochemistry staining of RUNX2. j Secretion of CXCL12 in the extract from neutrophils cultured on the glass (as Ctrl), SS, PT, SLA, and SR surfaces was detected by ELISA assay. k Representative images of the transwell assay. BMSCs were treated with neutrophil extracts with or without a CXCR3 receptor antagonist (SCH546738). Scale bar: 200 μm l Quantitative analysis of migrated cells among different groups. m Representative images of immunofluorescence staining showing the expression of CXCR3 of BMSCs after 24 h cultured with neutrophils extracts. Scale bar: 20 μm; 100 μm (insert). n Semiquantitative analysis of the mean immunofluorescence intensity of CXCR3. o Western blotting of CXCR3 and β-Actin of BMSCs after 24 h cultured with neutrophils extracts. p Quantitative analysis of the relative level of CXCR3/β-Actin.

neutrophils in the osseointegration of implants is still unclear. Combining the result of flow cytometry with scRNA seq, it was hypothesized that neutrophils might play a major regulatory role in early bone formation after implantation. To testify that, the circulating neutrophils (anti-Ly6G) were depleted in recipient mice for further experiments (Figs. S8b–S8d).

Our results confirmed that the depletion of neutrophils was detrimental to the bone regenerative process. Fourteen days post-implantation, the bone formation was evaluated via microcomputed tomography (μCT) (Fig. S8e) and histological observation. Neutropenia diminished new bone formation around SLA and SR implants (Fig. 7d), with a decrease in bone volume/total volume (BV/TV%) and trabecular thickness (Tb.Th.) (Fig. 7e and f). Meanwhile, compared with the N−/− group, the Masson staining slices (Fig. 7g) of control group had a larger new bone area and higher expression of RUNX2 protein (Fig. 7h and i).

Our previous study demonstrated that Sr^{2+} promoted the expression of CXCL12 [66], and current analysis showed that CXCL12-CXCR3 was the top 10 ligand-receptor pairs between neutrophils and HSCs (Fig. 7c). Further assays were performed to examine the effect of Sr^{2+} ions on the secretion of the CXCL12 from neutrophils. The release of CXCL12 from neutrophils cultured on the implant surfaces was evaluated by ELISA. Results revealed a significant increase of CXCL12 in cells cultured with SR surface compared with SS and control groups (Fig. 7j). Although there was no statistical difference among titanium-based implants, there was a slight increase in SR group when compared with PT and SLA group.

Next, to confirm the role of CXCR3 receptor in BMSCs recruitment, extracts of neutrophil cultures on different surfaces were collected for transwell assay. More BMSCs migrated to the lower chamber loaded with SR extract (Fig. 7k). The number of migrated cells was consistent with the concentration of CXCL12 in extracts. Enhanced cell migration induced by neutrophil extracts was attenuated by the CXCR3 receptor antagonist (SCH546738) (Fig. 7l). In addition, it was observed that neutrophil extracts from SR implant increased the expression level of the CXCR3 in BMSCs by immunofluorescence staining and western blotting (Fig. 7m–p). In summary, neutrophils played a promotive role in osseointegration, possibly enhancing bone formation by secreting CXCL12 which promotes the recruitment of BMSCs via the CXCR3 receptor of BMSCs.

4. Discussion

Bone healing process is typically considered the phases of blood-material interaction, provisional matrix formation, acute inflammation, chronic inflammation, foreign body reaction, and fibrous capsule formation or osseointegration. Three days after implantation was a point of innate immune response. Implanted biomaterials indispensably induced an intensive immune response compared to sham sites, but ideal biomaterials such as titanium-based implants also promoted osteogenic response, while relatively poor materials followed severe defense reactions and inflammation.

As the initial effector, neutrophils are rapidly recruited to the damage site and pre-regulated the local inflammatory state for recruiting and activating subsequent cells [69]. Ideal biomaterials, such as titanium implants, are surrounded by a certain proportion of neutrophils with highly differentiated phenotypes (G3, G4). Instead, the SS implant was infiltrated with excessive immature neutrophils (G0, G1, G2). More mature neutrophils such as G3 cells are more actively involved in the ROS biosynthetic process, which is a key biological mechanism regulating the survival, self-renewal, osteogenic differentiation, and matrix mineralization of MSCs [70]. Transient increases in ROS levels have been shown to induce G1/S phase transition, which plays a catalytic role in MSCs activation [71]. In osteogenic precursor cells, osteogenic induction upregulates BMP-2 signaling-mediated NAD(P)H oxidase activation, thereby generating mild levels of ROS to promote osteoblast differentiation [72]. In addition, physiological levels of ROS can activate the expression of extracellular signal-related kinases ERK1/2 and OPN in osteoblasts, thus supporting the extracellular matrix mineralization process [73].

In fact, neutrophils play a two-sided role in bone biology. In rheumatoid arthritis (RA), activated neutrophils expressed RANKL stimulated bone resorption in the inflamed joint [74]. Infiltrating neutrophils release neutrophil extracellular traps (NETs) containing carbamylated proteins enhanced pathogenic immune responses and promoted osteoclastogenesis in $CD14^{+}$ monocytes [75]. However, chemotactic neutrophils defects or neutropenia can rapidly induce inflammatory periodontal bone loss, and the extravasation ability of neutrophils appears to be essential for periodontal tissue homeostasis [76]. Neutrophils co-culture with MSCs can influence the differentiation of MSCs into osteoblasts by altering levels of IL-1α and TGF-β [77]. Thus, Neutrophils express and secrete cytokines or inflammatory mediators that can directly or indirectly affect bone homeostasis.

At the same time, neutrophils release MIP-1α, MIP-1β, and IFN-γ to induce more macrophages recruitment for phagocytosis [78]. The uptake of apoptotic neutrophils leads to M2-type in macrophages. However, the excessive production of MPO after NETs formation is phagocytosed by macrophages, leading to the release of ROS and more pro-inflammatory factors of macrophages, and then tends to M1 transformation [79,80]. Besides the traditional macrophage polarization, S100a8 is an endogenous TLR4 ligand involved in intercellular calcium homeostasis [81]. But when S100a8 is released slowly extracellular, its production exhibits strong pro-inflammatory properties that aggravate osteoarthritis pathology [82]. Therefore, the proportion of $S100a8^{hi}$ subcluster was positively correlated with the degree of the inflammatory response. $FcgR1^{hi}$ subcluster highly expressed *FcgR1*, which is the most important Fc receptor that promotes their role as scavenger cells that involve in phagocytosis and antigen presentation [83]. It follows that macrophages exhibit various heterogeneity under the regulation of different implant materials and play diverse roles in bone regeneration.

An intriguing finding is that SR implant surface was mostly new bone contact, while SS implant-bone marrow interface was surrounded by numerous FBGCs, more osteoclasts, and collagen fibers. The buildup of osseointegration seems to be FBR equilibrium, and the failure to establish this balance may lead to peri-implant bone loss or fibrosis. A

previous study found osteoclasts generated from classical/intermediate monocytes rather than non-classical monocytes in the presence of IL-17a *in vitro* [84]. The "non-classical" osteoclasts that shared numerous characteristics and physiological features (multinucleated and TRAP-positive) with osteoclasts but were unable to resorb bone, which generated from non-classical monocytes were considered to be FBGCs [85,86]. In this study, the expression of osteoclastogenic genes was increased in classical/intermediate monocytes, and the transcriptional level of FBGCs-related genes was higher in non-classical monocytes. Meanwhile, more non-classical monocytes formed in SS group, which was consistent with the number of FBGCs eventually formed. It was seen that biomaterials affect the differentiation trend of monocytes, and they are closely related to the multinucleated cell formation accompanied by biomaterials.

After the inflammatory initiation at the implant site, more immune cells are recruited to involve in foreign body response and bone regenerative process. An unexpected cluster of macDCs exhibited a mature phenotype with poor immune tolerance, mostly in SS implant rather than titanium-based implants. Typical immature DCs have low immunogenicity and strong antigen-presenting capacity, which may induce mild inflammation [87]. In addition, DCs play a central role in connecting the innate and adaptive immune systems [88]. Although this was early in implantation, our analysis could not illuminate the effect of different implant materials on B cells and T cells differentiation. The role of adaptive cells in bone regeneration cannot be denied. B cells express and secrete factors that control the critical RANKL/RANK/OPG axis of the interaction between bone cells and immunocytes [89,90]. As for T cells, they also affect bone healing by regulating the balance between their subclusters (e.g., Th1/Th2 and Treg/Th17) and other immune cells (e.g., B cells) [91,92]. In a mouse periodontitis model, the poly nanofibrous spongy microspheres lead to Treg enrichment, expansion, and Treg-mediated immune response against bone loss [93]. Biomaterial scaffolds enhanced the development of a pro-regenerative immune environment by implicating Th2 cells [16]. A recent study discovered a phenomenon that titanium-based implants establish a local microenvironment via recruitment of myeloid cells to induce T cell exhaustion, and exhibit a chronic inflamed and immunosuppressive status [94]. Thus, the effect of biomaterial properties on adaptive cell typing needs to be further studied.

Unlike previous literature, we sequenced all cells surrounding the implant without sorting, most of the cells were innate cells and adaptive cells, and only a cluster of HSCs with high expression of osteogenic genes and osteogenic differentiation potential was found (Fig. S7a). Hence, immunocytes play a critical role in pre-molding a biomaterial-based osteoimmune microenvironment, and the interactions between immune cells and HSCs are inseparable. It is believed that the essence of osseointegration is due to the effective homing and osteogenic differentiation of stem cells on the implant surface. Current results confirmed the promotive role of neutrophils in the new bone formation and the recruitment of BMSCs after implantation. Neutrophils have pro-vascularization potential and improve the engraftment of bioengineered tissues [67,68]. In ectopic endochondral ossification, IL-8-induced neutrophils are recruited to the implantation site and promote chemotaxis of BMSCs by secreting SDF-1α [95].

Furthermore, neutrophils are sensitive to the properties of biomaterial and exhibit differential inflammatory responses to titanium surfaces. Sr-incorporated scaffold-induced neutrophils play an immunomodulatory role in promoting angiogenesis and soft tissue regeneration by down-regulating the NF-κB pathway and increasing the phosphorylation of STAT3 [14]. Our previous study also found that Sr^{2+} enhanced the CXCL12/CXCR4 signaling pathway *in vitro* and *in vivo*, which promoted the migration and osteogenic differentiation of BMSCs [66].

Consistent with the above results, our findings showed that SR implant promoted the secretion of CXCL12 in neutrophils compared with the control group, whereas SS implant inhibited that. The top ligand-receptor pairs between neutrophils and stem cells indicated the potential role of the CXCL12/CXCR3 signal axis. CXCR3 presents similar transmembrane helices and different conformations of terminal regions as CXCR4 [96]. CXCR3 ligands also synergize with CXCL12 to induce cell migration that reflects a synergic relationship of the CXCL12/CXCR3 [97]. SR extracts activated the CXCR3 receptor in BMSCs, and the CXCR3 receptor antagonist attenuated Sr^{2+}-induced increased BMSCs recruitment. Thus, the above evidence demonstrated that neutrophils play a promotive role in implant osseointegration, and one of the possible reasons is the enhanced recruitment of BMSCs via the CXCL12/CXCR3 axis. However, due to the complexity of the osteoimmune microenvironment, we also realized that SR promotes BMSCs recruitment not only by secreting more CXCL12 but also by other factors. Preliminary detection of cytokines contained in the supernatant released by neutrophils, and found some differentially expressed cytokines between SR and SS surfaces, such as IL-1β, IL-6, IFN-γ, IL-10, and MIP-3a (Fig. S9), which need further explored.

5. Conclusion

In conclusion, the network of communication between immunocytes and bone tissue surrounding the implant is complex and delicate. First, a preliminary description of the osteoimmune microenvironment revealed that both innate and adaptive cells influence osseointegration (Fig. 8a). Different implant materials affect immune cell differentiation and heterogeneity, resulting in long-term clinical function. Second, SS implants were accompanied by excessive neutrophils and $S100a8^{hi}$ macrophages, leading to an aggressive immune response, inflammatory cell infiltration, and eventual fibrous capsule formation instead of osseointegration. Conversely, SR implants were surrounded by an appropriate amount of mature G3 neutrophils and highly differentiated macrophages, achieving the foreign body equilibrium and functional integration under moderate immune response (Fig. 8b). Finally, the promotive role of neutrophils in the osseointegration of implants is elucidated, which may improve bone formation by enhancing the recruitment of BMSCs via the CXCL12/CXCR3 signal axis.

Our findings contribute to a better knowledge of osteoimmunology and are valuable for the design and modification of 'osteoimmune-smart' biomaterials in the field of bone regeneration. However, one of the study's limitations lies in the incomplete understanding of the effects of biomaterial modification on the differentiation and biological functions of adaptive immune cells. And, because the detection time point was short, the subtypes of osteogenic progenitors were not well characterized. We need to extend the postoperative time point and further analyze the effect of biomaterials on the differentiation and function of adaptive immune cells and osteogenic progenitors. In addition, another issue is a lack of sufficient disclosure about how neutrophils regulate bone regeneration. The close interactions among biomaterials, immunocytes, and bone tissue require further investigation.

Ethics approval statement

All the experiments were approved by the Institutional Animal Care and Use Committee of Zhejiang University, Hangzhou, China (ZJU20220152).

CRediT authorship contribution statement

Jia Li: Conceptualization, Writing – original draft, contributed to conception, design, and drafted the manuscript, Data curation, Funding acquisition, Formal analysis, contributed to the data acquisition and analysis, All authors have read and approved the final version of the manuscript. **Congrui Zhao:** Data curation, Funding acquisition, Formal analysis, contributed to the data acquisition and analysis, All authors have read and approved the final version of the manuscript. **Yangbo Xu:** Data curation, Funding acquisition, Formal analysis, contributed to the

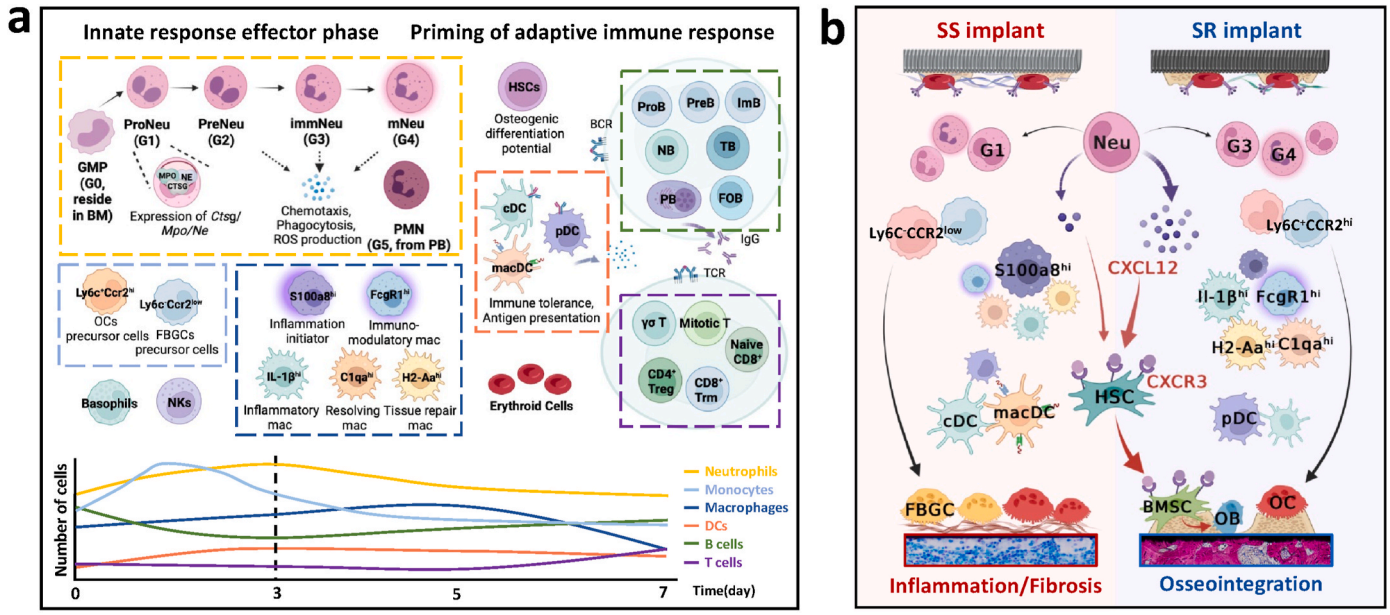

Fig. 8. Cell mapping centered on the osteoimmune microenvironment after implantation.
a Sc-RNA seq analysis of cell heterogeneity and temporal changes in the osteoimmune microenvironment after implantation. b Bone immune responses and prognosis of SS and SR implants. In this figure, major differences in innate immune cell subclusters were shown. Neutrophils may promote the effective homing of BMSCs through the CXCL12-CXCR3 signaling axis. OC: osteoclast; OB: osteoblast; FBGC: foreign body giant cell; BMSC: bone mesenchymal stem cell.

data acquisition and analysis, All authors have read and approved the final version of the manuscript. **Lu Song:** contributed to the animal model establishment and sample collection, All authors have read and approved the final version of the manuscript. **Yanqi Chen:** contributed to the animal model establishment and sample collection, All authors have read and approved the final version of the manuscript. **Yuzi Xu:** contributed to the animal model establishment and sample collection, All authors have read and approved the final version of the manuscript. **Yang Ma:** contributed to the revision of the manuscript, All authors have read and approved the final version of the manuscript. **Siyuan Wang:** contributed to the animal model establishment and sample collection, All authors have read and approved the final version of the manuscript. **Antian Xu:** Conceptualization, Writing – original draft, contributed to conception, design, and drafted the manuscript, contributed to the revision of the manuscript, All authors have read and approved the final version of the manuscript. **Fuming He:** Conceptualization, Writing – original draft, contributed to conception, design, and drafted the manuscript, contributed to the revision of the manuscript, All authors have read and approved the final version of the manuscript.

Declaration of competing interest

The authors declare that they have no known competing financial interests or personal relationships that could have appeared to influence the work reported in this paper.

Acknowledgements

The study was supported by grants from the National Natural Science Foundation of China (No. 82271026) and the Key Research and Development Program of Science and Technology Department of Zhejiang Province (No. 2019C03081).

Appendix A. Supplementary data

Supplementary data to this article can be found online at https://doi.org/10.1016/j.bioactmat.2022.10.009.

References

[1] J.L. Wang, J.K. Xu, C. Hopkins, D.H. Chow, L. Qin, Biodegradable magnesium-based implants in orthopedics-A general review and perspectives, Adv. Sci. 7 (2020), 1902443, https://doi.org/10.1002/advs.201902443.
[2] R. Trindade, T. Albrektsson, P. Tengvall, A. Wennerberg, Foreign body reaction to biomaterials: on mechanisms for buildup and breakdown of osseointegration, Clin. Implant Dent. Relat. Res. 18 (2016) 192–203, https://doi.org/10.1111/cid.12274.
[3] K. Ley, M1 means kill; M2 means heal, J. Immunol. 199 (2017) 2191–2193, https://doi.org/10.4049/jimmunol.1701135.
[4] Z.G. Fridlender, J. Sun, S. Kim, V. Kapoor, G. Cheng, L. Ling, G.S. Worthen, S. M. Albelda, Polarization of tumor-associated neutrophil phenotype by TGF-beta: "N1" versus "N2" TAN, Cancer Cell 16 (2009) 183–194, https://doi.org/10.1016/j.ccr.2009.06.017.
[5] E. Olmsted-Davis, J. Mejia, E. Salisbury, Z. Gugala, A.R. Davis, A population of M2 macrophages associated with bone formation, Front. Immunol. 12 (2021), 686769, https://doi.org/10.3389/fimmu.2021.686769.
[6] P. Zhou, D. Xia, Z. Ni, T. Ou, Y. Wang, H. Zhang, L. Mao, K. Lin, S. Xu, J. Liu, Calcium silicate bioactive ceramics induce osteogenesis through oncostatin M, Bioact. Mater. 6 (2021) 810–822, https://doi.org/10.1016/j.bioactmat.2020.09.018.
[7] M. Tsukasaki, H. Takayanagi, Osteoimmunology: evolving concepts in bone-immune interactions in health and disease, Nat. Rev. Immunol. 19 (2019) 626–642, https://doi.org/10.1038/s41577-019-0178-8.
[8] O. Veiseh, J.C. Doloff, M. Ma, A.J. Vegas, H.H. Tam, A.R. Bader, J. Li, E. Langan, J. Wyckoff, W.S. Loo, S. Jhunjhunwala, A. Chiu, S. Siebert, K. Tang, J. Hollister-Lock, S. Aresta-Dasilva, M. Bochenek, J. Mendoza-Elias, Y. Wang, M. Qi, D. M. Lavin, M. Chen, N. Dholakia, R. Thakrar, I. Lacik, G.C. Weir, J. Oberholzer, D. L. Greiner, R. Langer, D.G. Anderson, Size- and shape-dependent foreign body immune response to materials implanted in rodents and non-human primates, Nat. Mater. 14 (2015) 643–651, https://doi.org/10.1038/nmat4290.
[9] S. Hosseinpour, L.J. Walsh, C. Xu, Modulating osteoimmune responses by mesoporous silica nanoparticles, ACS Biomater. Sci. Eng. (2021), https://doi.org/10.1021/acsbiomaterials.1c00899.
[10] W. Qiao, D. Pan, Y. Zheng, S. Wu, X. Liu, Z. Chen, M. Wan, S. Feng, K.M.C. Cheung, K.W.K. Yeung, X. Cao, Divalent metal cations stimulate skeleton interoception for new bone formation in mouse injury models, Nat. Commun. 13 (2022) 535, https://doi.org/10.1038/s41467-022-28203-0.
[11] T. Wang, J. Bai, M. Lu, C. Huang, D. Geng, G. Chen, L. Wang, J. Qi, W. Cui, L. Deng, Engineering immunomodulatory and osteoinductive implant surfaces via mussel adhesion-mediated ion coordination and molecular clicking, Nat. Commun. 13 (2022) 160, https://doi.org/10.1038/s41467-021-27816-1.
[12] Y. Feng, Q. Li, D. Wu, Y. Niu, C. Yang, L. Dong, C. Wang, A macrophage-activating, injectable hydrogel to sequester endogenous growth factors for in situ angiogenesis, Biomaterials 134 (2017) 128–142, https://doi.org/10.1016/j.biomaterials.2017.04.042.
[13] A.T. Xu, Y.W. Xie, J.G. Xu, J. Li, H. Wang, F.M. He, Effects of strontium-incorporated micro/nano rough titanium surfaces on osseointegration via

modulating polarization of macrophages, Colloids Surf. B Biointerfaces 207 (2021), 111992, https://doi.org/10.1016/j.colsurfb.2021.111992.
[14] T. Li, H. He, Z. Yang, J. Wang, Y. Zhang, G. He, J. Huang, D. Song, J. Ni, X. Zhou, J. Zhu, M. Ding, Strontium-doped gelatin scaffolds promote M2 macrophage switch and angiogenesis through modulating the polarization of neutrophils, Biomater. Sci. 9 (2021) 2931–2946, https://doi.org/10.1039/d0bm02126a.
[15] X. Zheng, F. Zhou, Y. Gu, X. Duan, A. Mo, Effect of different titanium surfaces on maturation of murine bone marrow-derived dendritic cells, Sci. Rep. 7 (2017), 41945, https://doi.org/10.1038/srep41945.
[16] K. Sadtler, K. Estrellas, B.W. Allen, M.T. Wolf, H. Fan, A.J. Tam, C.H. Patel, B. S. Luber, H. Wang, K.R. Wagner, J.D. Powell, F. Housseau, D.M. Pardoll, J. H. Elisseeff, Developing a pro-regenerative biomaterial scaffold microenvironment requires T helper 2 cells, Science 352 (2016) 366–370, https://doi.org/10.1126/science.aad9272.
[17] E. Papalexi, R. Satija, Single-cell RNA sequencing to explore immune cell heterogeneity, Nat. Rev. Immunol. 18 (2018) 35–45, https://doi.org/10.1038/nri.2017.76.
[18] Y. Chen, X.Y. Chen, J.W. Shen, F.M. He, W. Liu, The characterization and osteogenic activity of nanostructured strontium-containing oxide layers on titanium surfaces, Int. J. Oral Maxillofac. Implants 31 (2016) e102–e115, https://doi.org/10.11607/jomi.4415.
[19] A. Vishwakarma, N.S. Bhise, M.B. Evangelista, J. Rouwkema, M.R. Dokmeci, A. M. Ghaemmaghami, N.E. Vrana, A. Khademhosseini, Engineering immunomodulatory biomaterials to tune the inflammatory response, Trends Biotechnol. 34 (2016) 470–482, https://doi.org/10.1016/j.tibtech.2016.03.009.
[20] D.E. Muench, A. Olsson, K. Ferchen, G. Pham, R.A. Serafin, S. Chutipongtanate, P. Dwivedi, B. Song, S. Hay, K. Chetal, L.R. Trump-Durbin, J. Mookerjee-Basu, K. Zhang, J.C. Yu, C. Lutzko, K.C. Myers, K.L. Nazor, K.D. Greis, D.J. Kappes, S. S. Way, N. Salomonis, H.L. Grimes, Mouse models of neutropenia reveal progenitor-stage-specific defects, Nature 582 (2020) 109–114, https://doi.org/10.1038/s41586-020-2227-7.
[21] M. Evrard, I.W.H. Kwok, S.Z. Chong, K.W.W. Teng, E. Becht, J. Chen, J.L. Sieow, H. L. Penny, G.C. Ching, S. Devi, J.M. Adrover, J.L.Y. Li, K.H. Liong, L. Tan, Z. Poon, S. Foo, J.W. Chua, I.H. Su, K. Balabanian, F. Bachelerie, S.K. Biswas, A. Larbi, W.Y. K. Hwang, V. Madan, H.P. Koeffler, S.C. Wong, E.W. Newell, A. Hidalgo, F. Ginhoux, L.G. Ng, Developmental analysis of bone marrow neutrophils reveals populations specialized in expansion, trafficking, and effector functions, Immunity 48 (2018) 364–379, https://doi.org/10.1016/j.immuni.2018.02.002, e368.
[22] X. Xie, Q. Shi, P. Wu, X. Zhang, H. Kambara, J. Su, H. Yu, S.Y. Park, R. Guo, Q. Ren, S. Zhang, Y. Xu, L.E. Silberstein, T. Cheng, F. Ma, C. Li, H.R. Luo, Single-cell transcriptome profiling reveals neutrophil heterogeneity in homeostasis and infection, Nat. Immunol. 21 (2020) 1119–1133, https://doi.org/10.1038/s41590-020-0736-z.
[23] I. Kwok, E. Becht, Y. Xia, M. Ng, Y.C. Teh, L. Tan, M. Evrard, J.L.Y. Li, H.T.N. Tran, Y. Tan, D. Liu, A. Mishra, K.H. Liong, K. Leong, Y. Zhang, A. Olsson, C.K. Mantri, P. Shyamsunder, Z. Liu, C. Piot, C.A. Dutertre, H. Cheng, S. Bari, N. Ang, S. K. Biswas, H.P. Koeffler, H.L. Tey, A. Larbi, I.H. Su, B. Lee, A. St John, J.K.Y. Chan, W.Y.K. Hwang, J. Chen, N. Salomonis, S.Z. Chong, H.L. Grimes, B. Liu, A. Hidalgo, E.W. Newell, T. Cheng, F. Ginhoux, L.G. Ng, Combinatorial single-cell analyses of granulocyte-monocyte progenitor heterogeneity reveals an early uni-potent neutrophil progenitor, Immunity 53 (2020) 303–318, https://doi.org/10.1016/j.immuni.2020.06.005, e305.
[24] A. Sheshachalam, N. Srivastava, T. Mitchell, P. Lacy, G. Eitzen, Granule protein processing and regulated secretion in neutrophils, Front. Immunol. 5 (2014) 448, https://doi.org/10.3389/fimmu.2014.00448.
[25] S.M. Lawrence, R. Corriden, V. Nizet, The ontogeny of a neutrophil: mechanisms of granulopoiesis and homeostasis, Microbiol. Mol. Biol. Rev. 82 (2018), https://doi.org/10.1128/MMBR.00057-17.
[26] T.A. Wynn, K.M. Vannella, Macrophages in tissue repair, regeneration, and fibrosis, Immunity 44 (2016) 450–462, https://doi.org/10.1016/j.immuni.2016.02.015.
[27] W. Yao, Y. Chen, Z. Li, J. Ji, A. You, S. Jin, Y. Ma, Y. Zhao, J. Wang, L. Qu, H. Wang, C. Xiang, S. Wang, G. Liu, F. Bai, L. Yang, Single cell RNA sequencing identifies a unique inflammatory macrophage subset as a druggable target for alleviating acute kidney injury, Adv. Sci. (2022), e2103675, https://doi.org/10.1002/advs.202103675.
[28] T.R. Hammond, C. Dufort, L. Dissing-Olesen, S. Giera, A. Young, A. Wysoker, A. J. Walker, F. Gergits, M. Segel, J. Nemesh, S.E. Marsh, A. Saunders, E. Macosko, F. Ginhoux, J. Chen, R.J.M. Franklin, X. Piao, S.A. McCarroll, B. Stevens, Single-cell RNA sequencing of microglia throughout the mouse lifespan and in the injured brain reveals complex cell-state changes, Immunity 50 (2019) 253–271, https://doi.org/10.1016/j.immuni.2018.11.004, e256.
[29] K.J. Mould, N.D. Jackson, P.M. Henson, M. Seibold, W.J. Janssen, Single cell RNA sequencing identifies unique inflammatory airspace macrophage subsets, JCI Insight 4 (2019), https://doi.org/10.1172/jci.insight.126556.
[30] U.M. Gundra, N.M. Girgis, D. Ruckerl, S. Jenkins, L.N. Ward, Z.D. Kurtz, K. E. Wiens, M.S. Tang, U. Basu-Roy, A. Mansukhani, J.E. Allen, P. Loke, Alternatively activated macrophages derived from monocytes and tissue macrophages are phenotypically and functionally distinct, Blood 123 (2014) e110–e122, https://doi.org/10.1182/blood-2013-08-520619.
[31] J. Schott, S. Reitter, J. Philipp, K. Haneke, H. Schafer, G. Stoecklin, Translational regulation of specific mRNAs controls feedback inhibition and survival during macrophage activation, PLoS Genet. 10 (2014), e1004368, https://doi.org/10.1371/journal.pgen.1004368.
[32] P. Ma, P. Zhang, S. Chen, W. Shi, J. Ye, S. Chen, R. Ju, B. Liu, Y. Zheng, Y. Liu, Immune cell landscape of patients with diabetic macular edema by single-cell RNA analysis, Front. Pharmacol. 12 (2021), 754933, https://doi.org/10.3389/fphar.2021.754933.
[33] Y. Bi, J. Chen, F. Hu, J. Liu, M. Li, L. Zhao, M2 macrophages as a potential target for antiatherosclerosis treatment, Neural Plast. (2019), 6724903, https://doi.org/10.1155/2019/6724903, 2019.
[34] R. Shechter, O. Miller, G. Yovel, N. Rosenzweig, A. London, J. Ruckh, K.W. Kim, E. Klein, V. Kalchenko, P. Bendel, S.A. Lira, S. Jung, M. Schwartz, Recruitment of beneficial M2 macrophages to injured spinal cord is orchestrated by remote brain choroid plexus, Immunity 38 (2013) 555–569, https://doi.org/10.1016/j.immuni.2013.02.012.
[35] S. Sprangers, T.J. de Vries, V. Everts, Monocyte heterogeneity: consequences for monocyte-derived immune cells, J Immunol Res (2016), 1475435, https://doi.org/10.1155/2016/1475435, 2016.
[36] J. Gamrekelashvili, R. Giagnorio, J. Jussofie, O. Soehnlein, J. Duchene, C. G. Briseno, S.K. Ramasamy, K. Krishnasamy, A. Limbourg, T. Kapanadze, C. Ishifune, R. Hinkel, F. Radtke, L.J. Strobl, U. Zimber-Strobl, L.C. Napp, J. Bauersachs, H. Haller, K. Yasutomo, C. Kupatt, K.M. Murphy, R.H. Adams, C. Weber, F.P. Limbourg, Regulation of monocyte cell fate by blood vessels mediated by Notch signalling, Nat. Commun. 7 (2016), 12597, https://doi.org/10.1038/ncomms12597.
[37] S. Yona, K.W. Kim, Y. Wolf, A. Mildner, D. Varol, M. Breker, D. Strauss-Ayali, S. Viukov, M. Guilliams, A. Misharin, D.A. Hume, H. Perlman, B. Malissen, E. Zelzer, S. Jung, Fate mapping reveals origins and dynamics of monocytes and tissue macrophages under homeostasis, Immunity 38 (2013) 79–91, https://doi.org/10.1016/j.immuni.2012.12.001.
[38] L. Ziegler-Heitbrock, The CD14+ CD16+ blood monocytes: their role in infection and inflammation, J. Leukoc. Biol. 81 (2007) 584–592, https://doi.org/10.1189/jlb.0806510.
[39] R.J. Miron, H. Zohdi, M. Fujioka-Kobayashi, D.D. Bosshardt, Giant cells around bone biomaterials: osteoclasts or multi-nucleated giant cells? Acta Biomater. 46 (2016) 15–28, https://doi.org/10.1016/j.actbio.2016.09.029.
[40] S.K. Wculek, F.J. Cueto, A.M. Mujal, I. Melero, M.F. Krummel, D. Sancho, Dendritic cells in cancer immunology and immunotherapy, Nat. Rev. Immunol. 20 (2020) 7–24, https://doi.org/10.1038/s41577-019-0210-z.
[41] Y. Yang, X. Wang, R.J. Miron, X. Zhang, The interactions of dendritic cells with osteoblasts on titanium surfaces: an in vitro investigation, Clin. Oral Invest. 23 (2019) 4133–4143, https://doi.org/10.1007/s00784-019-02852-w.
[42] P.M. Kou, Z. Schwartz, B.D. Boyan, J.E. Babensee, Dendritic cell responses to surface properties of clinical titanium surfaces, Acta Biomater. 7 (2011) 1354–1363, https://doi.org/10.1016/j.actbio.2010.10.020.
[43] T. Nikolic, M. Bunk, H.A. Drexhage, P.J. Leenen, Bone marrow precursors of nonobese diabetic mice develop into defective macrophage-like dendritic cells in vitro, J. Immunol. 173 (2004) 4342–4351, https://doi.org/10.4049/jimmunol.173.7.4342.
[44] M. Guilliams, C.A. Dutertre, C.L. Scott, N. McGovern, D. Sichien, S. Chakarov, S. Van Gassen, J. Chen, M. Poidinger, S. De Prijck, S.J. Tavernier, I. Low, S.E. Irac, C.N. Mattar, H.R. Sumatoh, G.H.L. Low, T.J.K. Chung, D.K.H. Chan, K.K. Tan, T.L. K. Hon, E. Fossum, B. Bogen, M. Choolani, J.K.Y. Chan, A. Larbi, H. Luche, S. Henri, Y. Saeys, E.W. Newell, B.N. Lambrecht, B. Malissen, F. Ginhoux, Unsupervised high-dimensional analysis aligns dendritic cells across tissues and species, Immunity 45 (2016) 669–684, https://doi.org/10.1016/j.immuni.2016.08.015.
[45] Y.M.H. Kimura*, F. Takeshita*, L.E. Takaokay, M. Matsuokaz, M. Makino*, Upregulation of T-cell-stimulating activity of mycobacteria-infected macrophages, Scand. J. Immunol. 60 (2004) 278–286, https://doi.org/10.1111/j.0300-9475.2004.01472.x.
[46] L. Zhang, Z. Li, K.M. Skrzypczynska, Q. Fang, W. Zhang, S.A. O'Brien, Y. He, L. Wang, Q. Zhang, A. Kim, R. Gao, J. Orf, T. Wang, D. Sawant, J. Kang, D. Bhatt, D. Lu, C.M. Li, A.S. Rapaport, K. Perez, Y. Ye, S. Wang, X. Hu, X. Ren, W. Ouyang, Z. Shen, J.G. Egen, Z. Zhang, X. Yu, Single-cell analyses inform mechanisms of myeloid-targeted therapies in colon cancer, Cell 181 (2020) 442–459 e429, https://doi.org/10.1016/j.cell.2020.03.048.
[47] L. Zhao, Y. Li, T. Xu, Q. Lv, X. Bi, X. Liu, G. Fu, Y. Zou, J. Ge, Z. Chen, W. Zhang, Dendritic cell-mediated chronic low-grade inflammation is regulated by the RAGE-TLR4-PKCbeta1 signaling pathway in diabetic atherosclerosis, Mol Med 28 (2022) 4, https://doi.org/10.1186/s10020-022-00431-6.
[48] A.F. Zahorchak, C. Macedo, D.E. Hamm, L.H. Butterfield, D.M. Metes, A. W. Thomson, High PD-L1/CD86 MFI ratio and IL-10 secretion characterize human regulatory dendritic cells generated for clinical testing in organ transplantation, Cell. Immunol. 323 (2018) 9–18, https://doi.org/10.1016/j.cellimm.2017.08.008.
[49] C. Zhu, G. Chen, Y. Zhao, X.M. Gao, J. Wang, Regulation of the development and function of B cells by ZBTB transcription factors, Front. Immunol. 9 (2018) 580, https://doi.org/10.3389/fimmu.2018.00580.
[50] J. Wang, Y. Xu, Z. Chen, J. Liang, Z. Lin, H. Liang, Y. Xu, Q. Wu, X. Guo, J. Nie, B. Lu, B. Huang, H. Xian, X. Wang, Q. Wu, J. Zeng, C. Chai, M. Zhang, Y. Lin, L. Zhang, S. Zhao, Y. Tong, L. Zeng, X. Gu, Z.G. Chen, S. Yi, T. Zhang, D. Delfouneso, Y. Zhang, S.L. Nutt, A.M. Lew, L. Lu, F. Bai, H. Xia, Z. Wen, Y. Zhang, Liver immune profiling reveals pathogenesis and therapeutics for biliary atresia, Cell 183 (2020) 1867–1883, https://doi.org/10.1016/j.cell.2020.10.048, e1826.
[51] H. Wang, H.C. Morse 3rd, S. Bolland, Transcriptional control of mature B cell fates, Trends Immunol. 41 (2020) 601–613, https://doi.org/10.1016/j.it.2020.04.011.
[52] S. Zehentmeier, J.P. Pereira, Cell circuits and niches controlling B cell development, Immunol. Rev. 289 (2019) 142–157, https://doi.org/10.1111/imr.12749.
[53] D. Toben, I. Schroeder, T. El Khassawna, M. Mehta, J.E. Hoffmann, J.T. Frisch, H. Schell, J. Lienau, A. Serra, A. Radbruch, G.N. Duda, Fracture healing is

accelerated in the absence of the adaptive immune system, J. Bone Miner. Res. 26 (2011) 113–124, https://doi.org/10.1002/jbmr.185.
[54] M. Shapiro-Shelef, K. Calame, Regulation of plasma-cell development, Nat. Rev. Immunol. 5 (2005) 230–242, https://doi.org/10.1038/nri1572.
[55] K. Hirota, J.H. Duarte, M. Veldhoen, E. Hornsby, Y. Li, D.J. Cua, H. Ahlfors, C. Wilhelm, M. Tolaini, U. Menzel, A. Garefalaki, A.J. Potocnik, B. Stockinger, Fate mapping of IL-17-producing T cells in inflammatory responses, Nat. Immunol. 12 (2011) 255–263, https://doi.org/10.1038/ni.1993.
[56] T. Ono, K. Okamoto, T. Nakashima, T. Nitta, S. Hori, Y. Iwakura, H. Takayanagi, IL-17-producing gammadelta T cells enhance bone regeneration, Nat. Commun. 7 (2016), 10928, https://doi.org/10.1038/ncomms10928.
[57] M. Ono, Control of regulatory T-cell differentiation and function by T-cell receptor signalling and Foxp3 transcription factor complexes, Immunology 160 (2020) 24–37, https://doi.org/10.1111/imm.13178.
[58] I. Raphael, S. Nalawade, T.N. Eagar, T.G. Forsthuber, T cell subsets and their signature cytokines in autoimmune and inflammatory diseases, Cytokine 74 (2015) 5–17, https://doi.org/10.1016/j.cyto.2014.09.011.
[59] S. Li, J. Wan, W. Anderson, H. Sun, H. Zhang, X. Peng, Z. Yu, T. Wang, X. Yan, W. Smith, Downregulation of IL-10 secretion by Treg cells in osteoarthritis is associated with a reduction in Tim-3 expression, Biomed. Pharmacother. 79 (2016) 159–165, https://doi.org/10.1016/j.biopha.2016.01.036.
[60] Y. Gao, F. Grassi, M.R. Ryan, M. Terauchi, K. Page, X. Yang, M.N. Weitzmann, R. Pacifici, IFN-gamma stimulates osteoclast formation and bone loss in vivo via antigen-driven T cell activation, J. Clin. Invest. 117 (2007) 122–132, https://doi.org/10.1172/JCI30074.
[61] E.V. Shashkova, J. Trivedi, A.B. Cline-Smith, C. Ferris, Z.S. Buchwald, J. Gibbs, D. Novack, R. Aurora, Osteoclast-primed Foxp3+ CD8 T cells induce T-bet, eomesodermin, and IFN-gamma to regulate bone resorption, J. Immunol. 197 (2016) 726–735, https://doi.org/10.4049/jimmunol.1600253.
[62] H. Chen, J. Wu, L. Lu, Z. Hu, X. Li, L. Huang, X. Zhang, M. Chen, X. Qin, L. Xie, Identification of hub genes associated with immune infiltration and predict prognosis in hepatocellular carcinoma via bioinformatics approaches, Front. Genet. 11 (2020), 575762, https://doi.org/10.3389/fgene.2020.575762.
[63] M. Efremova, M. Vento-Tormo, S.A. Teichmann, R. Vento-Tormo, (2019). 10.1101/680926..
[64] M. Kondo, A.J. Wagers, M.G. Manz, S.S. Prohaska, D.C. Scherer, G.F. Beilhack, J. A. Shizuru, I.L. Weissman, Biology of hematopoietic stem cells and progenitors: implications for clinical application, Annu. Rev. Immunol. 21 (2003) 759–806, https://doi.org/10.1146/annurev.immunol.21.120601.141007.
[65] B. Sacchetti, A. Funari, S. Michienzi, S. Di Cesare, S. Piersanti, I. Saggio, E. Tagliafico, S. Ferrari, P.G. Robey, M. Riminucci, P. Bianco, Self-renewing osteoprogenitors in bone marrow sinusoids can organize a hematopoietic microenvironment, Cell 131 (2007) 324–336, https://doi.org/10.1016/j.cell.2007.08.025.
[66] C. Zhou, A.T. Xu, D.D. Wang, G.F. Lin, T. Liu, F.M. He, The effects of Sr-incorporated micro/nano rough titanium surface on rBMSC migration and osteogenic differentiation for rapid osteointegration, Biomater. Sci. 6 (2018) 1946–1961, https://doi.org/10.1039/c8bm00473k.
[67] R.Z. Lin, C.N. Lee, R. Moreno-Luna, J. Neumeyer, B. Piekarski, P. Zhou, M. A. Moses, M. Sachdev, W.T. Pu, S. Emani, J.M. Melero-Martin, Host non-inflammatory neutrophils mediate the engraftment of bioengineered vascular networks, Nat Biomed Eng 1 (2017), https://doi.org/10.1038/s41551-017-0081.
[68] T.D.K. Herath, A. Larbi, S.H. Teoh, C.J. Kirkpatrick, B.T. Goh, Neutrophil-mediated enhancement of angiogenesis and osteogenesis in a novel triple cell co-culture model with endothelial cells and osteoblasts, J Tissue Eng Regen Med 12 (2018) e1221–e1236, https://doi.org/10.1002/term.2521.
[69] T. Nemeth, M. Sperandio, A. Mocsai, Neutrophils as emerging therapeutic targets, Nat. Rev. Drug Discov. 19 (2020) 253–275, https://doi.org/10.1038/s41573-019-0054-z.
[70] Q. Li, Z. Gao, Y. Chen, M.X. Guan, The role of mitochondria in osteogenic, adipogenic and chondrogenic differentiation of mesenchymal stem cells, Protein Cell 8 (2017) 439–445, https://doi.org/10.1007/s13238-017-0385-7.
[71] O.G. Lyublinskaya, Y.G. Borisov, N.A. Pugovkina, I.S. Smirnova, J.V. Obidina, J. S. Ivanova, V.V. Zenin, A.N. Shatrova, A.V. Borodkina, N.D. Aksenov, V.I. Zemelko, E.B. Burova, M.V. Puzanov, N.N. Nikolsky, Reactive oxygen species are required for human mesenchymal stem cells to initiate proliferation after the quiescence exit, Oxid. Med. Cell. Longev. (2015), 502105, https://doi.org/10.1155/2015/502105, 2015.
[72] C.C. Mandal, S. Ganapathy, Y. Gorin, K. Mahadev, K. Block, H.E. Abboud, S. E. Harris, G. Ghosh-Choudhury, N. Ghosh-Choudhury, Reactive oxygen species derived from Nox4 mediate BMP2 gene transcription and osteoblast differentiation, Biochem. J. 433 (2011) 393–402, https://doi.org/10.1042/BJ20100357.
[73] S. Khalid, H. Yamazaki, M. Socorro, D. Monier, E. Beniash, D. Napierala, Reactive oxygen species (ROS) generation as an underlying mechanism of inorganic phosphate (Pi)-induced mineralization of osteogenic cells, Free Radic. Biol. Med. 153 (2020) 103–111, https://doi.org/10.1016/j.freeradbiomed.2020.04.008.
[74] A. Chakravarti, M.A. Raquil, P. Tessier, P.E. Poubelle, Surface RANKL of Toll-like receptor 4-stimulated human neutrophils activates osteoclastic bone resorption, Blood 114 (2009) 1633–1644, https://doi.org/10.1182/blood-2008-09-178301.
[75] L.J. O'Neil, A. Barrera-Vargas, D. Sandoval-Heglund, J. Merayo-Chalico, C. Carmona-Rivera, Neutrophil-mediated carbamylation promotes articular damage in rheumatoid arthritis, Sci. Adv. (44) (2020) 6. 10.1126:sciadv.abd2688.pdf.
[76] N.M. Moutsopoulos, J. Konkel, M. Sarmadi, M.A. Eskan, T. Wild, N. Dutzan, L. Abusleme, C. Zenobia, K.B. Hosur, T. Abe, G. Uzel, W. Chen, T. Chavakis, S. M. Holland, G. Hajishengallis, Defective neutrophil recruitment in leukocyte adhesion deficiency type I disease causes local IL-17-driven inflammatory bone loss, Sci. Transl. Med. 6 (2014), https://doi.org/10.1126/scitranslmed.3007696, 229ra240.
[77] A. Al-Hakami, S.Q. Alqhatani, S. Shaik, S.M. Jalfan, M.S.A. Dhammam, W. Asiri, A. M. Alkahtani, A. Devaraj, H.C. Chandramoorthy, Cytokine physiognomies of MSCs from varied sources confirm the regenerative commitment post-coculture with activated neutrophils, J. Cell. Physiol. 235 (2020) 8691–8701, https://doi.org/10.1002/jcp.29713.
[78] K.C. Navegantes, R. de Souza Gomes, P.A.T. Pereira, P.G. Czaikoski, C.H. M. Azevedo, M.C. Monteiro, Immune modulation of some autoimmune diseases: the critical role of macrophages and neutrophils in the innate and adaptive immunity, J. Transl. Med. 15 (2017) 36, https://doi.org/10.1186/s12967-017-1141-8.
[79] D. Nakazawa, H. Shida, Y. Kusunoki, A. Miyoshi, S. Nishio, U. Tomaru, T. Atsumi, A. Ishizu, The responses of macrophages in interaction with neutrophils that undergo NETosis, J. Autoimmun. 67 (2016) 19–28, https://doi.org/10.1016/j.jaut.2015.08.018.
[80] C. Song, H. Li, Y. Li, M. Dai, L. Zhang, S. Liu, H. Tan, P. Deng, J. Liu, Z. Mao, Q. Li, X. Su, Y. Long, F. Lin, Y. Zeng, Y. Fan, B. Luo, C. Hu, P. Pan, NETs promote ALI/ARDS inflammation by regulating alveolar macrophage polarization, Exp. Cell Res. 382 (2019), 111486, https://doi.org/10.1016/j.yexcr.2019.06.031.
[81] S. Wang, R. Song, Z. Wang, Z. Jing, S. Wang, J. Ma, S100A8/A9 in inflammation, Front. Immunol. 9 (2018) 1298, https://doi.org/10.3389/fimmu.2018.01298.
[82] W. de Munter, E.J. Geven, A.B. Blom, B. Walgreen, M.M. Helsen, L.A. Joosten, J. Roth, T. Vogl, F.A. van de Loo, M.I. Koenders, W.B. van den Berg, P.M. van der Kraan, P.L. van Lent, Synovial macrophages promote TGF-beta signaling and protect against influx of S100A8/S100A9-producing cells after intra-articular injections of oxidized low-density lipoproteins, Osteoarthritis Cartilage 25 (2017) 118–127, https://doi.org/10.1016/j.joca.2016.07.020.
[83] C. Rosales, Fcgamma receptor heterogeneity in leukocyte functional responses, Front. Immunol. 8 (2017) 280, https://doi.org/10.3389/fimmu.2017.00280.
[84] S. Sprangers, T. Schoenmaker, Y. Cao, V. Everts, T.J. de Vries, Different blood-borne human osteoclast precursors respond in distinct ways to IL-17a, J. Cell. Physiol. 231 (2016) 1249–1260, https://doi.org/10.1002/jcp.25220.
[85] T.J. de Vries, I. El Bakkali, T. Kamradt, G. Schett, I.D.C. Jansen, P. D'Amelio, What are the peripheral blood determinants for increased osteoclast formation in the various inflammatory diseases associated with bone loss? Front. Immunol. 10 (2019) 505, https://doi.org/10.3389/fimmu.2019.00505.
[86] B. ten Harkel, T. Schoenmaker, D.I. Picavet, N.L. Davison, T.J. de Vries, V. Everts, The foreign body giant cell cannot resorb bone, but dissolves hydroxyapatite like osteoclasts, PLoS One 10 (2015), e0139564, https://doi.org/10.1371/journal.pone.0139564.
[87] H.C. Probst, S. Muth, H. Schild, Regulation of the tolerogenic function of steady-state DCs, Eur. J. Immunol. 44 (2014) 927–933, https://doi.org/10.1002/eji.201343862.
[88] J. Constantino, C. Gomes, A. Falcao, B.M. Neves, M.T. Cruz, Dendritic cell-based immunotherapy: a basic review and recent advances, Immunol. Res. 65 (2017) 798–810, https://doi.org/10.1007/s12026-017-8931-1.
[89] R.P. Settem, K. Honma, S. Chinthamani, T. Kawai, A. Sharma, B-cell RANKL contributes to pathogen-induced alveolar bone loss in an experimental periodontitis mouse model, Front. Physiol. 12 (2021), 722859, https://doi.org/10.3389/fphys.2021.722859.
[90] Y. Li, G. Toraldo, A. Li, X. Yang, H. Zhang, W.P. Qian, M.N. Weitzmann, B cells and T cells are critical for the preservation of bone homeostasis and attainment of peak bone mass in vivo, Blood 109 (2007) 3839–3848, https://doi.org/10.1182/blood-2006-07-037994.
[91] Y. Liu, L. Wang, T. Kikuiri, K. Akiyama, C. Chen, X. Xu, R. Yang, W. Chen, S. Wang, S. Shi, Mesenchymal stem cell-based tissue regeneration is governed by recipient T lymphocytes via IFN-gamma and TNF-alpha, Nat. Med. 17 (2011) 1594–1601, https://doi.org/10.1038/nm.2542.
[92] H.Y. Dar, A. Singh, P. Shukla, R. Anupam, R.K. Mondal, P.K. Mishra, R. K. Srivastava, High dietary salt intake correlates with modulated Th17-Treg cell balance resulting in enhanced bone loss and impaired bone-microarchitecture in male mice, Sci. Rep. 8 (2018) 2503, https://doi.org/10.1038/s41598-018-20896-y.
[93] Z. Liu, X. Chen, Z. Zhang, X. Zhang, L. Saunders, Y. Zhou, P.X. Ma, Nanofibrous spongy microspheres to distinctly release miRNA and growth factors to enrich regulatory T cells and rescue periodontal bone loss, ACS Nano 12 (2018) 9785–9799, https://doi.org/10.1021/acsnano.7b08976.
[94] Q. Fan, H. Dai, J. Bai, J. Xu, Q. Ma, Z. Fei, X. Zhou, K.W. Leong, C. Wang, Degradation-resistant implanted biomaterials establish an immunosuppressive microenvironment that induces T cell exhaustion by recruiting myeloid cells, Fundamental Research 2 (2022) 648–658, https://doi.org/10.1016/j.fmre.2021.10.007.
[95] B. Cai, D. Lin, Y. Li, L. Wang, J. Xie, T. Dai, F. Liu, M. Tang, L. Tian, Y. Yuan, L. Kong, S.G.F. Shen, N2-Polarized neutrophils guide bone mesenchymal stem cell recruitment and initiate bone regeneration: a missing piece of the bone regeneration puzzle, Adv. Sci. 8 (2021), e2100584, https://doi.org/10.1002/advs.202100584.
[96] S. Costantini, R. Raucci, T. De Vero, G. Castello, G. Colonna, Common structural interactions between the receptors CXCR3, CXCR4 and CXCR7 complexed with their natural ligands, CXCL11 and CXCL12, by a modeling approach, Cytokine 64 (2013) 316–321, https://doi.org/10.1016/j.cyto.2013.05.024.
[97] B. Vanbervliet, N. Bendriss-Vermare, C. Massacrier, B. Homey, O. de Bouteiller, F. Briere, G. Trinchieri, C. Caux, The inducible CXCR3 ligands control plasmacytoid

dendritic cell responsiveness to the constitutive chemokine stromal cell-derived factor 1 (SDF-1)/CXCL12, J. Exp. Med. 198 (2003) 823–830, https://doi.org/10.1084/jem.20020437.